POLITECNICO DI TORINO
Repository ISTITUZIONALE

Energy performance and climate control in mechanically ventilated greenhouses: A dynamic modelling-based assessment and investigation

(Article begins on next page)
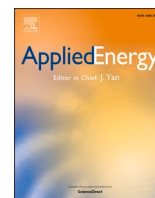
20 April 2024

Energy performance and climate control in mechanically ventilated greenhouses: A dynamic modelling-based assessment and investigation

Andrea Costantino [a,b], Lorenzo Comba [c,d], Giacomo Sicardi [e], Mauro Bariani [e], Enrico Fabrizio [a,*]

[a] DENERG, TEBE Research Group, Politecnico di Torino, Corso Duca degli Abruzzi 24, 10129 Torino, Italy
[b] Institute of Animal Science and Technology, Universitat Politècnica de València, Camino de Vera s/n, 46022 València, Spain
[c] DISAFA, University of Torino, Largo Paolo Braccini 2, 10095 Grugliasco (TO), Italy
[d] CNR-IEIIT, Politecnico di Torino, Corso Duca degli Abruzzi 24, 10129 Torino, Italy
[e] Munters Italy S.p.a., via Strada Piani 2, 18027 Chiusavecchia d'Imperia (IM), Italy

HIGHLIGHTS

- A new model for estimating the energy consumption of greenhouses is provided.
- A plant model is coupled to consider the crop effects on thermal and mass balances.
- The proposed model allows the user to simulate also variable angular speed fans.
- The model was successfully validated against real monitored data.
- Electrical energy consumption decreases by 25% using variable angular speed fans.

ARTICLE INFO

ABSTRACT

Controlled environment agriculture in greenhouse is a promising solution for meeting the increasing food demand of world population. The accurate control of the indoor environmental conditions proper of greenhouses enhances high crop productivity but, contemporarily, it entails considerable energy consumption due to the adoption of mechanical systems. This work presents a new modelling approach for estimating the energy consumption for climate control of mechanically ventilated greenhouses. The novelty of the proposed energy model lies in its integrated approach in simulating the greenhouse dynamics, considering the dynamic thermal and hygric behaviour of the building and the dynamic response of the cultivated crops to the variation of the solar radiation. The presented model simulates the operation of the systems and the energy performance, considering also the variable angular speed fans that are a new promising energy-efficient technology for this productive sector. The main outputs of the model are the hourly thermal and electrical energy use for climate control and the main indoor environmental conditions. The presented modelling approach was validated against a dataset acquired in a case study of a new fully mechanically controlled greenhouse during a long-term monitoring campaign. The present work contributes to increase the knowledge about the dynamics and the energy consumption of greenhouses, and it can be a valuable decision support tool for industry, farmers, and researchers to properly address an energy efficiency optimisation in mechanically ventilated greenhouses to reach the overall objective of decreasing the rising energy consumption of the agricultural sector.

1. Introduction

The last estimations of United Nations predict that world population could reach up to 10.1 billion of people in 2050 [1]. A similar demographical growth makes meeting the future food demand an issue of primary importance. Controlled Environment Agriculture (also known as protected agriculture) [2] may considerably contribute to meet the future food demand due to its high productivity [3]. The most widespread and efficient solutions for Controlled Environment Agriculture are greenhouses with a mechanical control of the indoor environment, focus of the present work. In this building type, in fact, climate control system manages the indoor environmental parameters (e.g. air temperature, relative humidity, CO_2 concentration and light) to provide the

Nomenclature

$\mathscr{A}, \widetilde{\mathscr{A}}$	Sets of simulated and measured values (indoor air temperature)	
$\mathscr{B}, \widetilde{\mathscr{B}}$	Sets of simulated and measured values (indoor relative humidity)	
$\mathscr{C}, \widetilde{\mathscr{C}}$	Sets of simulated and measured values (electrical energy consumption)	
A_{gh}	Greenhouse floor area [m^2]	
A_{gl}	Area of a surface of the greenhouse envelope [m^2]	
$a_{\text{flow}} - c_{\text{flow}}$	Regression coefficients for fan ventilation flow rate	
$a_{\text{perf}} - i_{\text{perf}}$	Regression coefficients for fan performance	
$\langle C_{\text{CO}_2\_i} \rangle$	Indoor CO_2 concentration [ppm]	
C_{gh}	Greenhouse heat capacity [kJ K^{-1}]	
c_{air}	Air specific heat capacity [J kg^{-1} K^{-1}]	
$Cv(RMSE)$	Coefficient of variation of the $RMSE$ [%]	
E_{el}	Electrical energy consumption [kWh]	
$E_{\text{el\_cool}}$	Electrical energy consumption for cooling ventilation [kWh]	
$E_{\text{el\_deh}}$	Electrical energy consumption for dehumidification [kWh]	
E_{th}	Thermal energy consumption [kWh]	
F_{v}	View factor [−]	
g_{sc}	Total solar transmission coefficient of the screen [−]	
$H_{\text{tr\_em}}$	Heat transfer coefficient [W K^{-1}]	
$H_{\text{tr\_fen}}$	Heat transfer coefficient [W K^{-1}]	
$H_{\text{tr\_is}}$	Heat transfer coefficient [W K^{-1}]	
$H_{\text{tr\_ms}}$	Heat transfer coefficient [W K^{-1}]	
$H_{\text{tr},1}$	Heat transfer coefficient [W K^{-1}]	
$H_{\text{tr},2}$	Heat transfer coefficient [W K^{-1}]	
$H_{\text{tr},3}$	Heat transfer coefficient [W K^{-1}]	
H_{ve}	Ventilation heat transfer coefficient [W K^{-1}]	
h_{t}	Sensible heat transfer coefficient due to transpiration [W m^{-2} K^{-1}]	
i	i-th fan of the greenhouse	
j	j-th simulation time-step	
k	k-th surface of the greenhouse envelope	
LAI	Leaf Area Index [m^2 m^{-2}]	
m_{LAI}	Slope of the LAI function [m^2 m^{-2}]	
$\dot{m}_{\text{vap}}$	Plant transpiration water vapour flow [mg$_{\text{vap}}$ m^{-2} s^{-1}]	
MBE	Mean Bias Error [%]	
n_{ach}	Ventilation air changes [h^{-1}]	
n_{fan}	Number of adopted fans	
n_{set}	Cardinality of a set of elements	
n_{sim}	Number of simulation time-steps	
n_{sur}	Number of envelope surfaces	
p_{atm}	Atmospheric pressure [Pa]	
p_{v}	Water vapour pressure [Pa]	
p_{vs}	Saturation water vapour pressure [Pa]	
q_{LAI}	y-intercept of LAI function [m^2 m^{-2}]	
R_{b}	Tipping coefficient of the solar radiation [−]	
RH_{i}	Indoor air relative humidity [%]	
$RH_{\text{i\_max}}$	Maximum indoor air relative humidity [%]	
RH_{o}	Outdoor air relative humidity [%]	
$RMSE$	Root Mean Square Error	
SFP	Specific fan performance [m^3 Wh^{-1}]	
SFP_{fix}	Specific fan performance of fixed angular speed fans [m^3 Wh^{-1}]	
SFP_{var}	Specific fan performance of variable angular speed fans [m^3 Wh^{-1}]	
$SHGC$	Solar Heat Gain Coefficient [−]	
$U-value$	Stationary thermal transmittance [W m^{-2} K^{-1}]	
V_{gh}	Greenhouse net volume [m^3]	

$\dot{V}_{\text{air}}$	Ventilation air flow [m^3 h^{-1}]	
$\dot{V}_{\text{cool}}$	Ventilation air flow for cooling [m^3 h^{-1}]	
$\dot{V}_{\text{deh}}$	Ventilation air flow for dehumidification [m^3 h^{-1}]	
$\dot{V}_{\text{fan\_fix}}$	Ventilation flow rate of fixed angular speed fans [m^3 h^{-1}]	
$\dot{V}_{\text{fan\_var}}$	Ventilation flow rate of variable angular speed fans [m^3 h^{-1}]	
$\dot{V}_{\text{inst}}$	Maximum greenhouse ventilation capacity [m^3 h^{-1}]	
VPD	Vapour Pressure Deficit [Pa]	
$x_{\text{air\_i}}$	Indoor air humidity ratio [g$_{\text{vap}}$ kg$_{\text{air}}$]	
$x_{\text{air\_i\_MAX}}$	Maximum indoor air humidity ratio [g$_{\text{vap}}$ kg$_{\text{air}}$]	
$x_{\text{air\_sup}}$	Supply air humidity ratio [g$_{\text{vap}}$ kg$_{\text{air}}$]	
z_{1-6}	Regression coefficients	
γ_{floor}	Calibration parameter for the floor [−]	
γ_{glass}	Calibration parameter for glazed surfaces [−]	
γ_{hig}	Calibration parameter for the greenhouse hygric capacity [−]	
$\gamma_{\text{m\_LAI}}$	Calibration parameter for LAI function slope [−]	
$\gamma_{\text{q\_LAI}}$	Calibration parameter for LAI function y-intercept [−]	
γ_{th}	Calibration parameter for the greenhouse thermal capacity [−]	
$\Delta\theta_{\text{air\_i}}$	Thermal gradient inside the greenhouse [°C]	
ΔE_{el}	Energy consumption deviation [%]	
Δp_{st}	Static pressure difference between inside and outside [Pa]	
$\Delta\tau$	Time step duration [s]	
δ	Dimensionless coefficient for plant transpiration [−]	
ε	Direct saturation effectiveness of the evaporative pads [−]	
η_{H}	Global efficiency of the heating system [−]	
$\theta_{\text{air\_i}}$	Indoor air temperature [°C]	
$\theta_{\text{air\_i(0)}}$	Indoor air temperature (0 W m^{-2} of heat load) [°C]	
$\theta_{\text{air\_i(10)}}$	Indoor air temperature (10 W m^{-2} of heat load) [°C]	
$\theta_{\text{air\_o}}$	Outdoor air temperature [°C]	
$\theta_{\text{air\_o\_db}}$	Dry-bulb temperature of outdoor air [°C]	
$\theta_{\text{air\_o\_wb}}$	Wet-bulb temperature of outdoor air [°C]	
$\theta_{\text{air\_sup}}$	Supply air temperature [°C]	
θ_{m}	Building mass temperature [°C]	
θ_{s}	Temperature of the indoor building surface [°C]	
$\theta_{\text{set\_C}}$	Air set point temperature for cooling [°C]	
$\theta_{\text{set\_H}}$	Air set point temperature for heating [°C]	
λ	Latent heat of vaporisation of water [MJ kg^{-1}]	
μ	Angle between beam solar radiation and the normal to the surface [°]	
ρ_{air}	Volumetric mass density of air [kg^3 m^3]	
σ	Psychrometric constant [Pa K^{-1}]	
τ	Time instant [s]	
$\phi_{\text{H/C\_nd}}$	Supplemental heat load for heating or cooling [W]	
$\phi_{\text{H/C\_nd(10)}}$	Heating or cooling load considering 10 W m^{-2} [W]	
ϕ_{ia}	Convective heat flow [W]	
ϕ_{im}	Radiative heat flow [W]	
$\phi_{\text{lat\_i}}$	Latent heat load due to plant transpiration [W]	
$\phi_{\text{m\_tot,j}}$	Total heat flow during the j-th hourly time-step [−]	
$\phi_{\text{sens\_i}}$	Solar sensible heat gain (after plant transpiration) [W]	
ϕ_{st}	Radiative heat flow [W]	
$\phi_{\text{sol\_b}}$	Beam outdoor solar radiation on horizontal plane [W m^{-2}]	
$\phi_{\text{sol\_d}}$	Diffuse outdoor solar radiation on horizontal plane [Wm^{-2}]	
$\phi_{\text{sol\_i}}$	Solar radiation that enters inside the greenhouse [W]	
$X, \widetilde{X}$	Simulated and measured generic time profiles	
$\chi_j, \widetilde{\chi}_j$	Simulated and measured generic value	
$\Psi, \widehat{\Psi}$	Initial and optimal set of calibration parameters	
$\Omega, \widehat{\Omega}$	Initial and optimal set of calibration parameters	
ω	Coefficient for water vapour sorption and storage [−]	

adequate indoor microclimate for crop growth also in climates and seasons in which the outfield cultivation would be otherwise impossible [3] (e.g. exotic plants can be cultivated at higher latitudes [4]). In this way, climate control of greenhouses enhances the possibility to cultivate crops near the locations of consumption, reducing the transportation with the related greenhouse gas emissions and the amount of food that perishes during this process [3].

The precise control of the indoor environmental conditions brings each plant to its genetic potential [5], increasing the quality and especially the quantity of the production [6]. It is estimated that the greenhouse yield referred to the unit of productive surface is between 10 [7] and 20 times higher than the open-field one [8]. For example, the yield of strawberry production is estimated to be 0.5 kg m^{-2} annum^{-1} in open fields, while in greenhouses it reaches 7.3 kg m^{-2} annum^{-1} [9]. Tomatoes can have an open-field yield of 7.5 kg m^{-2} annum^{-1}, while in greenhouses the yield exceeds 68 kg m^{-2} annum^{-1} [10]. The increased cultivation yield is possible at the expense of a considerable energy consumption due to climate control. The open-field cultivation of one kg of strawberries, for example, needs around 0.20 kWh considering both direct thermal and electrical energy (1 kWh = 3.6 MJ), while the open field cultivation of tomatoes needs 0.26 kWh kg^{-1}. When the cultivation of these crops is carried out in climate-controlled greenhouses, those energy consumptions dramatically increase, being 4.60 kWh kg^{-1} for strawberries and 17.50 kWh kg^{-1} for tomatoes (elaboration from [9,10]). These high energy consumptions make the greenhouse crop cultivation an energy-intensive activity in the framework of the agricultural industry [3]. According to International Energy Agency, in the Netherland (a country characterised by a high greenhouse production), the energy consumption of the agricultural sector is increasing due to the expansion of greenhouse crop cultivation [11].

Most of the energy consumption of greenhouses is due to heating which can need up to 530 kWh m^{-2} annum^{-1} in cool climates (such as the Scandinavian [12] and British one [13]) or up to 440 kWh m^{-2} annum^{-1} in warmer ones, such as in the Mediterranean area [12]. Heating represents between 65 and 85% of the total greenhouse energy consumption while the remaining share is due to electrical facilities, such as fans and actuators needed to cool the greenhouse [14]. The high solar radiation that enters the greenhouse through the glazed envelope, in fact, can considerably increase the indoor air temperature with detrimental effects for the cultivated crops. For this reason, cooling ventilation through fans and other cooling strategies [15] are adopted in greenhouse, increasing even more the energy needed by this building type. The high energy consumption that characterises greenhouse crop production is not only an environmental issue, but it considerably affects the production costs. The installation of the heating systems of greenhouses, in fact, represents between 30 and 60% of the total initial investment cost [16], while the use of energy is the second highest financial running cost after labour [3,14], accounting between 10 and 30% of the total cost of the production [12].

In this framework, the reduction of the energy demand of greenhouses can be identified as a key industry sustainable development goal [3] since it involves the three pillars of sustainability. Reducing this energy consumption, in fact, would increase the environmental sustainability (lower use of resource), the financial sustainability (lower financial cost) and social sustainability (higher food security). For this reason, a great attention is being paid on producing greenhouse crops in an energy-efficient manner [14], reducing the use of fossil fuels [8], replacing them by renewable energy sources through the use, for example, of heat pumps [17], biomass [18] or anaerobic digestion [12].

To do so, specific energy simulation models for greenhouses are needed since they make it possible to assess the effectiveness of energy-efficient solutions for greenhouse design and retrofit. The dynamic behaviour of greenhouse indoor climate is a combination of physical processes involving energy and mass transfer and is strongly affected by several time-varying features, such as the outside weather conditions,

the type and state of the cultivated crops, the adopted climate control system and its operation strategy [19]. The development of these models is a complex task because a normative framework lacks at European level. The European Union standard EN-13031-1 [20], in fact, provides only the rules for structural design and construction of greenhouses without giving any indications for the assessment of the greenhouse energy performance. In addition, ready to use building energy simulation tools such as TRNSYS and EnergyPlus are not suitable for simulating this building type since they do not adequately describe the physical processes of heat and mass transfer which occur in a greenhouse [21] and very complicated modifications are needed for this purpose [22]. For example, the effects of plant transpiration are omitted or excessively simplified connecting external models to the building energy simulation tool for simulating this phenomenon, but this solution does not make it possible to consider the plant-environment interaction. To fill this gap, several Authors in literature developed customized energy simulation models with different purposes. Most of these models are simplified in some features (e.g. control, modelling of the thermal inertia and system operation) or, on the contrary, are very complex. Complex models require several iterations that weigh the calculation down prevent them to be used to perform simulations in several scenarios characterized by different greenhouse configurations, an issue that considerably limits the use of these models among stakeholders (e.g. practitioners, farmers and industry). In addition, most of the already developed models enhance the improvement of the greenhouse energy performance optimizing the control strategy (operational stage), while few of them improve the energy performance focusing on an energy-efficient selection of the envelope and equipment during the design stage. The energy design of greenhouse, in fact, is usually a sort of "pre-selected scheme" in which fundamental issues such as the several possibilities that are provided by envelope and system technologies are not considered in detail. Reliable energy simulation models can break that "pre-selected scheme" since they can evaluate the effectiveness of new technologies and of innovative solutions, providing to stakeholders a clearer idea of the typical energy performance (and running cost) of the considered greenhouse, under typical conditions. Such simulation models, therefore, could significantly improve the energy design of new greenhouses and enhance the retrofit of old ones, increasing the energy saving and the crop production.

Objective of this work is to develop and validate a dynamic energy simulation model for assessing the indoor environmental conditions and the energy performance for climate control of fully-mechanically ventilated greenhouses. The present model is developed for being a decision support tool for stakeholders in the energy design and retrofit stages of greenhouses. The novelty of this work is to propose a reliable energy model able to simulate the greenhouse dynamics (e.g. thermal and hygric behaviour of the building, dynamic response of the crops) and the consequent dynamic response of the climate control systems. A deep attention is paid in modelling the climate control and the climate equipment that are mainly adopted in fully-mechanically ventilated greenhouses, in particular to variable angle speed fans. These equipment represent a new promising energy-efficient technology for the greenhouses sector, but reliable energy simulation models that integrate them are not present in literature. The present model integrates them (a novelty in literature), representing a first step toward the improvement of the knowledge about their effectiveness and their sizing.

The paper is organized as follows. The dynamics that characterise the indoor environment of a greenhouse that should be considered during the development of an energy simulation model of such enclosures are described in Section 2. In Section 3, the developed energy simulation model is described together with the different calculation modules and the relative equations. In Section 4, the reliability of the presented model is proved through a validation against a real dataset. In Section 5, the potentialities of the presented energy simulation model are highlighted through a numerical example comparing the indoor environmental conditions and energy performance of similar greenhouses in

different climate conditions. The concluding remarks are presented in Section 6.

2. Interactions between plants and the greenhouse enclosure

The energy modelling of greenhouses is challenging since this building type is characterised by peculiar features that are uncommon in other building types, such as the dimension of the enclosure, a total glazed envelope that entails high solar heat gains and high transmission heat losses. Furthermore, greenhouses are densely populated by plants that react in a specific way mainly to indoor air temperature (θ_{air_i}), relative humidity (RH_i), CO_2 concentration ($\langle C_{CO_2\_i} \rangle$), and solar radiation entering in the greenhouse (ϕ_{sol_i}) [3].

A fundamental interaction between plants and the greenhouse environment is plant transpiration, a process that converts between 30 and 50% of the incoming solar radiation into latent heat. The driver of the transpiration is the Vapour Pressure Deficit (*VPD*), with the "deficit" that is defined as the difference between the vapor pressure in the air and the saturated vapor pressure value. The smaller the difference, the more moisture-laden the air will be. The larger the difference, the drier the air will be. The use of *VPD* is widespread in the greenhouse production since this parameter is independent of θ_{air_i} and RH_i [23]. Crop foliage surface deeply affects the transpiration rate and its extension is evaluated through the Leaf Area Index (*LAI*), defined as leaf area per unit of greenhouse surface [24].

Active climate control systems enhance a precise control of the indoor climate conditions of the greenhouse. These systems provide supplemental heat through equipment such as gas air heaters or boilers. In this way, θ_{air_i} can be maintained over the minimum indoor air temperature (θ_{set_H}). On the contrary, mechanical cooling ventilation is activated when θ_{air_i} has to be maintained below a maximum indoor air temperature (θ_{set_C}). Cooling ventilation is supplied by a set of box or cone extraction fans provide a bay-flow or a cross-bay flow using outdoor fresh air maintaining the air speed below 0.75 m s^{-1} to avoid negative effects on CO_2 uptake of plants due to high air velocities [25]. Another strategy to decrease θ_{air_i} is the reduction of the solar radiation that enters inside the greenhouse (ϕ_{sol_i}). In greenhouses, the ϕ_{sol_i} is maximized during the cool season for enhancing plant photosynthesis and reducing the supplemental heating need, but it must be controlled during the warm season to avoid the overheating of the enclosure. For this purpose, reflective-diffusive screen systems, mixed glass-photovoltaic panels [26] or external film of calcium carbonate are adopted [27]. When cooling ventilation and solar radiation reduction are not enough to maintain θ_{air_i} below θ_{set_C}, evaporative cooling is adopted.

RH_i is another parameter that is carefully controlled inside greenhouses. RH_i is maintained above 50%, since lower RH_i values would increase the plant evaporation losses beyond its capacity of replacing the water lost, resulting in wilting, and burning of growing tips. Values of RH_i higher than 80%-90% should be avoided since they would favour the proliferation of fungal pathogenic organisms [25]. RH_i is controlled through extraction fans that are used to provide an airflow of fresh outdoor air that enters through a set of upper gable shutters automatically opened and closed to maintain a constant value of static pressure between inside and outside the greenhouse (Δp_{st}). In some situations, outdoor air can be characterized by a higher value of humidity ratio than indoor air. In these situations, ventilation cannot be used to decrease RH_i since to inlet outdoor air in the enclosure would further increase RH_i. Therefore, the only solution to decrease RH_i is the activation of the heating system: the increase of θ_{air_i} causes a consequent decrease of RH_i (the humidity ratio of indoor air remains constant in this psychrometric transformation).

The indoor CO_2 concentration ($\langle C_{CO_2\_i} \rangle$) is also controlled in greenhouses to avoid CO_2 compensation point of plants. This condition occurs when the amount of CO_2 absorbed by photosynthesis is the same released by plant respiration, with detrimental consequences for plant growth [28]. In greenhouses, $\langle C_{CO_2\_i} \rangle$ is maintained at adequate levels through ventilation with the exception of cold days in which CO_2 enrichment (a direct injection of CO_2 inside the enclosure) is preferred [29]. CO_2 enrichment is also performed to enhance plant growth over a normal level [29].

3. Model structure

3.1. Modelling background

As previously described, the dynamics inside a greenhouse are several and complex. The climate control systems that are adopted in greenhouses to control the indoor environmental conditions are different not only from the ones of other building types, but several differences can be found also between the ones of different types of greenhouses.

For these reasons, standardized calculation models for the estimation of the overall energy consumptions for climate control in greenhouses do not exist. On the contrary, various customized energy simulations models for this purpose have been developed, as described by the history of greenhouse model development presented in [30]. Analysing the recent scientific literature and the main reviews on this topic [3,31], different models developed for different and specific purposes can be found. Van Beveren et al. [32,33] developed a dynamic energy simulation model for optimizing the energy inputs of greenhouses working on the indoor environmental conditions. Lin et al. [34] applied the energy model developed by Van Beveren et al. [32,33] for improving the energy efficiency and the operating costs of Venlo-type greenhouses in South Africa analysing different control strategies. Chen et al. [35] developed a model for estimating the energy consumption of greenhouses through a model optimized prediction methodology in which the uncertain parameters of a physical model of the greenhouse were calibrated using optimization algorithms. Altes-Buch et al. [36] developed an open-source model in Modelica for simulating greenhouse climate and its complex interactions with thermal systems (e.g. CHP and heat pumps). Ahamed et al. [22] modelled the dynamic requirements of a solar greenhouse using TRNSYS and highlighting that this simulation tool is not suitable for simulating the greenhouse thermal environment since very complicated modifications are needed for this purpose. Similarly, Vadiee and Martin [8] developed an energy simulation model in TRNSYS to improve the overall energy performance of Swedish greenhouses. Taki et al. [37] developed a dynamic simulation model to estimate the indoor air temperature in six spots of the greenhouse with the aim of analysing the effects of thermal screen on the greenhouse energy consumption and on the indoor environmental conditions. Mobtaker et al. [38] developed a dynamic energy simulation model to predict the main greenhouse indoor temperature (e.g. air, soil and walls) with the aim of analysing the thermal energy losses and solar heat gains of different greenhouses shapes. A model for a similar purpose (the estimation of the main indoor temperatures of greenhouses) was developed by Joudi and Farhan [39], while the dynamic energy model of Reyes-Rosas et al. [40] was developed for a similar purpose (the estimation of greenhouse indoor air, soil and cover temperatures) but it was tailored for naturally ventilated greenhouses. Zhang et al. [41] developed a dynamic energy model in MATLAB environment that incorporates the dynamic absorbance and transmittance values of the greenhouse cover. Golzar et al. [31] proposed a coupled model to assess the greenhouse energy demand and crop yield for analysing with a high temporal resolution the potential of renewable energy use and the effects of different indoor environmental conditions on the crop yield. The work of Ward et al. [21] is different from other ones since it adopts the energy simulation model developed by Brown et al. [42] to analyse the retrofit opportunities for historic ornamental greenhouses (also known as "glasshouses") in United Kingdom. Recently, greenhouse energy models have been coupled with building energy model with the aim of

exploring the potentiality of Urban-Integrated

Agriculture. For example, Jans-Singh et al. [43] co-simulated a rooftop greenhouse integrated on the top of a school building. The co-simulation was performed through EnergyPlus (school building simulation) and a MATLAB model (greenhouse simulation). A similar analysis was carried out through WUFI commercial software by Gholami et al. [44]. These studies are of a foremost importance since they improve the integration of greenhouses in human buildings making it possible fine-tuning the exploitation of building waste streams (e.g. CO_2 and exhausted warm air) as input of the greenhouse and, contemporarily, to evaluate the extent to which greenhouses can contribute to decrease the building cooling and heating energy demand.

This literature analysis shows that different types of greenhouse energy simulation models are present in literature. Some models are mainly focused on estimating indoor temperatures (e.g. air and soil temperatures) while others aim at decreasing the energy consumption of greenhouses but, in many cases, they were tailored for a specific greenhouse. In addition, those models are to be used during the operative stage of the greenhouses, since they aim at optimizing the climate control strategies once selected a given envelope and climate control system. On the contrary, the energy simulation model that is presented in this work aims at improving the energy performance of the greenhouses through an energy energy conscious design and/or retrofit, enhancing the comparison between a wide range of configurations of envelope and systems of the considered greenhouse.

As just presented, several greenhouse energy simulation models developed for different purposes are present in literature. Despite the differences, all the energy simulation models for greenhouses can be grouped in three different categories, as reported in [3]: first-principle, data-driven and hybrid energy models, as schematized in Fig. 1.

First-principle energy models (also known as white-box models) relies on a mathematical set of physical and empirical equations that describe the thermal behaviour of the greenhouse. The development of a first-principle energy model depends on a deep knowledge of the system physics and of the properties of both envelope and HVAC system. A negative aspect of first-principle energy models is that a great effort is required in the calibration stage. Instead, data-driven energy models (also known as black-box models) avoid these problems since they are based on large datasets of real measured data that are used to formulate

a prediction using algorithms (such as Bayesian network [45] or machine learning [46]) to seek relations between input and output data. Data-driven energy models can simulate with a good accuracy the thermal behaviour of an existing building, but it is unsuitable for the design stage, since measured data are not available, and to obtain generalized results that does not refer to an existing case study. Hybrid energy models (also known as grey-box models) [47,48] are a compromise between the previously presented models (white-box models) since they rely on both physical equations and real datasets. The adoption of hybrid energy models represents an interesting choice when the knowledge of the problem physics is incomplete or there is a lack of data. Since the objective of this work is to develop an energy simulation model with a detailed modelling of HVAC system (especially for the new variable angular speed fans) to be used to obtain generalized results also for design purposes, data-driven and hybrid energy models are not considered the best solutions for the present work and first-principle energy models are preferred.

First-principle energy models (within which the presented model falls) can be divided in two subgroups: steady-state and dynamic energy models, as visible in the schematization of Fig. 1. The steady-state models, in turn, can be further classified in:

- fully-steady-state models;
- quasi-steady-state models.

Fully-steady-state models adopt a very large time-step (up to one month) and consider only the steady-state part of the energy balance equation, neglecting any transient term, such as the energy storage in the building thermal mass. Jolliet et al. [49] developed a steady-state model to study the thermal energy balance of greenhouses, that represented an intermediate solutions between very simple models of low precision and precise (but time consumptive) dynamic models. Singh and Tiwari [50] performed steady state analyses to determine the best shape of the greenhouses to maintain the adequate indoor air temperature and to minimize the energy consumptions. Campiotti et al. [51] developed a fully-steady-state model for greenhouses for calculating the reduction of the energy consumption in the framework of Italian legislation.

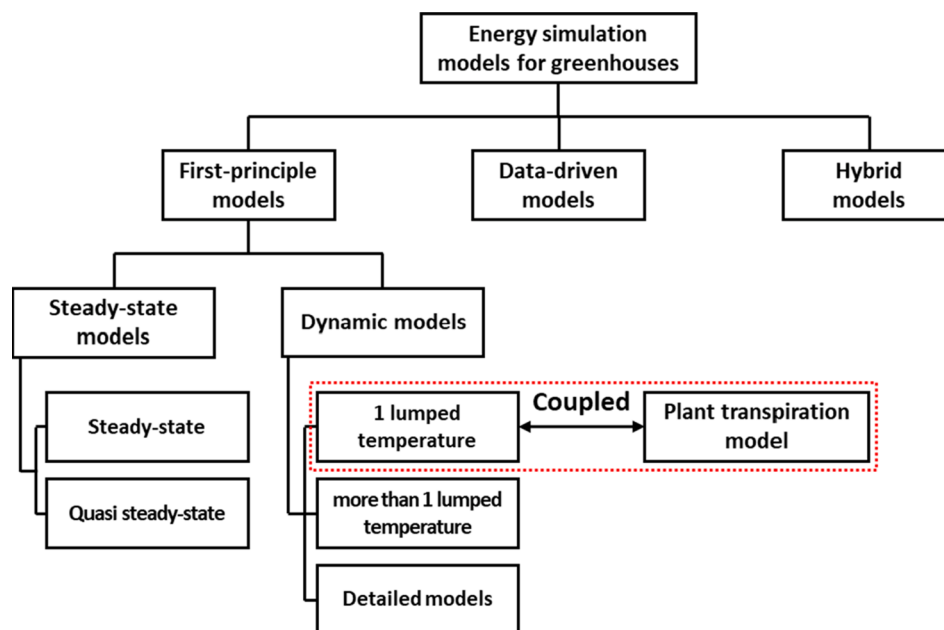The complexity of steady-state models increases in quasi-steady-state

Fig. 1. Classification (red dotted contour) of the energy simulation model presented in this work according to the existing literature. (For interpretation of the references to colour in this figure legend, the reader is referred to the web version of this article.)

models [52], since an adjusting parameter is introduced to consider the heat storage phenomenon.

Dynamic energy models are more complex to implement, are characterised by short time-steps (one hour or less) and provide more reliable results. They can be classified in:

- dynamic energy models with one lumped temperature;
- dynamic energy models with more than one lumped temperature;
- detailed dynamic simulation models.

Dynamic energy models with lumped temperatures (one or more) are usually customized models implemented in different codes to solve a set of energy balance equations [39]. In this type of energy model, HVAC system is usually not modelled in detail due to its complexity [3]. To enhance the simulation of HVAC systems, detailed dynamic simulations performed in Building Energy Simulation tools (BES), such as EnergyPlus and TRNSYS, are preferred. Chen et al. [53] developed a numerical model in EnergyPlus to study the thermal performance of a passive solar greenhouse. Rasheed et al. [54] developed a dynamic energy simulation model of a greenhouse to study the effect of screens (characterized by different materials and control strategies) on the thermal energy requirements of greenhouses. Bambara and Athienitis [55] developed a dynamic energy model of a greenhouse in TRNSYS to identify the most cost-effective cladding design for a specific greenhouse.

BES tools enable accurate simulation of the most common types of HVAC systems, but they are not suitable for simulating the greenhouse environment and the new technologies and HVAC systems typical of greenhouses, since they were developed for "civil" buildings and since their level of customizability is low [22,56]. Furthermore, BES tools do not account peculiar phenomena that usually take place inside greenhouses and strongly influence the energy balance, such as plant transpiration and plant growth. To consider the effects of these phenomena, models that simulate them are integrated into the energy model, originating the so-called coupled energy models [3,52].

In this framework, the energy model presented in this work can be classified as a first-principle coupled dynamic energy simulation model, as shown by the red dotted contour present in Fig. 1. This classification depends on the fact that the core of the developed model is a set of physical equations that are used for solving a dynamic energy balance characterised by one lumped temperature (θ_{air_i}). The presented model is also considered coupled since integrates a plant transpiration model for correctly setting the moisture balance and estimating the reduction of the solar radiation heat gain. Furthermore, in the present model the HVAC system is modelled in detail considering the presence of several equipment, with a particular focus on variable angular speed fans, a new energy-efficient technology that is spreading in greenhouses. The modelling of this technology is a novelty in literature.

3.2. Model workflow

The presented energy simulation model was developed in a spreadsheet environment and it is made by nine calculation modules that were developed for modelling all the relevant greenhouse subsystems and the plant transpiration. The developed calculation modules are the following:

- Preliminary calculation module
- Solar radiation module
- Plant transpiration module
- Thermal balance module
- Moisture balance module
- Heating system module
- Cooling pad efficiency module
- Dehumidification ventilation system module
- Cooling ventilation system module

The previously presented modules are organised as shown in Fig. 2, where the entire workflow of the developed simulation model is presented. Preliminary stage of the simulation is the user input of constant parameter (block "Input" in the workflow of Fig. 2), such as the thermophysical and optical properties of the envelope, the geographical location of the greenhouse and the climate control features (e.g. air set point temperatures and fan models). Some details about the crop type, such as the *LAI*, are also requested in this phase. In the following stage, the model starts with the "Preliminary calculations module" to determine all the variables that are needed for the subsequent steps, such as the heat transfer coefficients and the total building fabric heat capacity. After the preliminary calculations, a calculation loop (represented in Fig. 2 by a dotted contour) is repeated for each time-step of the simulation. Each loop begins with the calculations of the "Solar radiation module" aimed at determining the hourly solar angles to estimate the total solar radiation reaching the crops. This value is an input of the "Plant transpiration module" that estimates the rate of water vapor released by the crops and the reduction of sensible heat from solar radiation due to crop transpiration. Using these values, the sensible energy balance is solved ("Thermal balance module") for providing the inputs for the estimation of RH_i ("Moisture balance module"). If RH_i exceeds the maximum limit value (RH_{i_max}), the model calculates the needed dehumidification ventilation flow rate ($\dot{V}_{deh}$, in "Dehumidification ventilation system module") and then the electrical energy consumption for dehumidification. The obtained $\dot{V}_{deh}$ is used to update the thermal and moisture balances. If RH_i is below the limit, the model evaluates if θ_{air_i} is between θ_{set_H} and θ_{set_C}. If θ_{air_i} falls in this range, neither heating nor cooling is needed and θ_{air_i} is in free-floating conditions. If θ_{air_i} falls out of the range and heating is needed ($\theta_{air\_i} < \theta_{set\_H}$), the model updates the thermal balance, calculates the theoretical thermal energy need ("Heating system module") and the actual thermal energy consumption (considering the heating system efficiency). If cooling is needed ($\theta_{air\_i} > \theta_{set\_C}$), the model updates the thermal balance, calculating the cooling load that has to be provided to the greenhouses to reach θ_{set_C}. This estimated cooling load is only theoretical since the model considers that no mechanical cooling system is present in the simulated greenhouse and θ_{air_i} is decreased using cooling ventilation. For this reason, the obtained theoretical cooling load is converted in a ventilation air flow rate ("Cooling ventilation system module") considering also the activation of evaporative pads ("Cooling pad efficiency module"). After this stage, the actual electrical energy consumption is calculated, and the current iteration of the loop calculation ends. The loop, starting from the "Solar radiation module", is thus repeated for the following hourly step. In the meanwhile, the thermal and electrical energy consumption calculated at each time-step are integrated along the simulation time period, to obtain the yearly thermal and electrical energy consumptions. Hourly time profiles of θ_{air_i} and RH_i are additional valuable outputs of the model.

In the following sections, more details and the major equations of the main calculation modules are presented.

3.3. Calculation modules

3.3.1. Preliminary calculation module

In the preliminary calculation module, all the variables needed for the following calculations are calculated starting from the input data. Among the most important variables that are calculated in this module, the heat transfer coefficients needed to solve the thermal balance can be mentioned.

3.3.2. Solar radiation module

This module estimates the actual solar radiation ϕ_{sol_i} that enters inside the greenhouse and can reach the crop canopies. The timely solar position in the sky is calculated (using the solar equations of [57]) with the aim of considering in the model the effect of the optical properties of
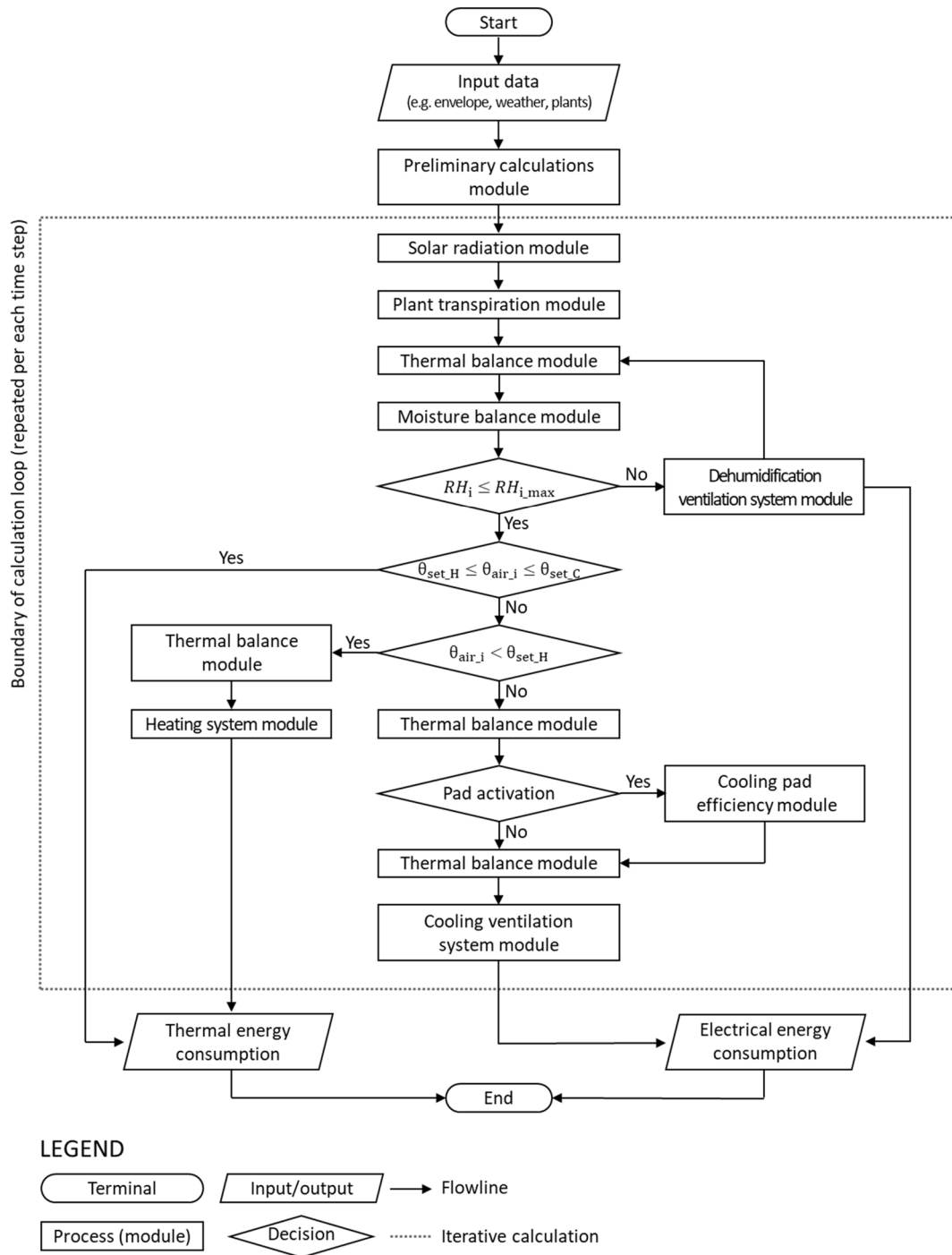
Fig. 2. Model workflow through the calculation modules. The dotted contour represents the calculation loop that is repeated for each time-step of the simulation.

the glazed envelope as a function of the angle of incidence of solar radiation on the glazed surface. Furthermore, in this way, the effect of eventual solar screens can be properly modelled, considering that they can be opened or closed depending on the solar radiation intensity.

At time-step *j*, the total solar radiation that enters in the greenhouse $\phi_{\text{sol\_i,j}}$ is calculated as

$$\phi_{\text{sol\_i,j}} = \sum_{k=1}^{n_{\text{sur}}} \left\{ A_{\text{gl,k}} \cdot g_{\text{sc,j}} \cdot \left[\phi_{\text{sol\_b,j}} \cdot R_{\text{b,k}}(\mu_{\text{j}}) \cdot SHGC_{\text{k}}(\mu_{\text{j}}) \right. \right.$$
$$\left. \left. + \phi_{\text{sol\_d,j}} \cdot F_{\text{v,k}}(\mu_{\text{j}}) \cdot SHGC_{\text{k}}(\mu_{\text{j}}) \right] \right\} \quad [\text{W}] \tag{1}$$

where $A_{\text{gl,k}}$ is the generic *k*-th surface of the glazed envelope exposed to

the solar radiation, n_{sur} is the total number of these surfaces, $g_{\text{sc,j}}$ is the total solar transmission coefficient of the screen (dimensionless) at the *j*-th time-step (the screen can be opened or closed), while $\phi_{\text{sol\_b,j}}$ and $\phi_{\text{sol\_d,j}}$ are the beam and diffuse solar radiation on the horizontal external plane (W m^{-2}), respectively, at the considered time-step. The tipping coefficient $R_{\text{b,k}}$ (dimensionless) identifies the rate between the solar radiation hitting a generically oriented surface *k* and the solar radiation on a horizontal plane. The term $F_{\text{v,k}}$ is the view factor (dimensionless) between a generically oriented surface *k* of the envelope and the sky. The term $SHGC_{\text{k}}$ (dimensionless) is the Solar Heat Gain Coefficient that estimates the total thermal solar radiation that crosses the glazed surface *k*. In Eq. (1), the terms $R_{\text{b,k}}$, $F_{\text{v,k}}$ and $SHGC_{\text{k}}$ are expressed as function of

μ_j, that represents the angle between the direction of the beam solar radiation and the normal to the glazed surface calculated in the *j*-th time-step.

3.3.3. Plant transpiration module

This calculation module aims at estimating the amount of water vapour that is transpired by the cultivated crops. This is a crucial aspect to be considered when a greenhouse is analysed from the thermal and hygrometric point of view since plant transpiration considerably affects the greenhouse thermal and moisture balances.

Plant transpiration is a complex phenomenon that is related to several parameters, such as the stomatal resistance [58]. In literature, several plant transpiration models were proposed, such as the Stanghellini's one [59], the "big leaf" model of Penman-Monteith [60,61], models based on new algorithms (such as the random forest regression one [62]) or models that estimates the effects of transpiration starting from the outdoor conditions [63]. Even though several models to predict transpiration of greenhouse crops are present in literature, is still not clear which model is more appropriate [64]. Among them, the Stanghellini's model [59] is one of the most established and widely used. In this work, the latent heat released by the crop due to transpiration is calculated through a rearrangement of the diffusion equation. The resistances to diffusion were modelled as a function of the indoor environmental conditions inside the greenhouse, described by the already cited quantities $\phi_{\text{sol\_i}}$, $\theta_{\text{air\_i}}$, $\langle C_{\text{CO}_2\text{\_i}} \rangle$ and *VPD*. Stanghellini's model has been proven to be highly accurate, but it requires to solve a convergence problem that involves complex computation and numerous inputs, requiring a considerable computing time. For this reason, the simplified model by Jolliet [65] was implemented in this work, being an effective trade-off between affordable computing time and accuracy of results. This latter transpiration model was obtained by linearizing the Stanghellini's one according to the method proposed in [66] that consists in a non-linear regression on the results obtained with the Stanghellini's model and a set of 168 different boundary conditions obtained varying $\phi_{\text{sol\_i}}$, *VPD* and *LAI*. The results of this linearization of Stanghellini's model show that transpiration can be approximated with a good accuracy through Eq. (2). At each analysed time-step *j*, the plant transpiration water vapour flow ($\dot{m}_{\text{vap}}$) per unit of cultivated area is calculated as

$$\dot{m}_{\text{v,j}} = \frac{\delta}{\lambda} \cdot \frac{\phi_{\text{sol\_i,j}}}{A_{\text{gh}}} + \frac{h_{\text{t,j}}}{\lambda \cdot \sigma} \cdot VPD_j \quad \left[\frac{\text{mg}_{\text{vap}}}{\text{m}^2\text{s}} \right] \tag{2}$$

where λ is the latent heat of vaporisation of water (2.5 MJ kg^{-1} at 20 °C), σ is a psychrometric constant (66 Pa K^{-1}) and *VPD* is calculated as

$$VPD_j = p_{\text{vs,j}} - p_{\text{v,j}} \quad \text{[Pa]} \tag{3}$$

where $p_{\text{vs,j}}$ is the saturation water vapour pressure and $p_{\text{v,j}}$ is the water vapour pressure at time-step *j*, both expressed in Pa. The term A_{gh} is the greenhouse floor area (input data) expressed in m^2. The term δ is a dimensionless coefficient that characterises the influence of $\phi_{\text{sol\_i}}$ on transpiration, while $h_{\text{t,j}}$ is the sensible heat transfer coefficient due to transpiration. These coefficients are calculated as

$$\delta = z_1 \cdot \ln\left(1 + z_2 \cdot LAI_j^{z_3}\right) \quad [-] \tag{4}$$

$$h_{\text{t,j}} = z_4 \cdot LAI_j \cdot \left(1 - z_5 \cdot e^{\left(-\frac{\phi_{\text{sol\_i,j}}}{z_6}\right)}\right) \quad \left[\frac{\text{W}}{\text{m}^2\text{K}}\right] \tag{5}$$

where $z_1 - z_6$ are the regression coefficients reported in Table 1. The term LAI_j represents the *LAI* of the crops present inside the greenhouse at the *j*-th time step of the simulation. The presented energy model, in fact, simulates the plant growth linearly varying the *LAI* during the crop production cycle.

In Fig. 3, an example of calculation of $\dot{m}_{\text{vap}}$ according to Eq. (5) was

Table 1
Regression coefficients of Eqs. (4) and (5) used in this work.

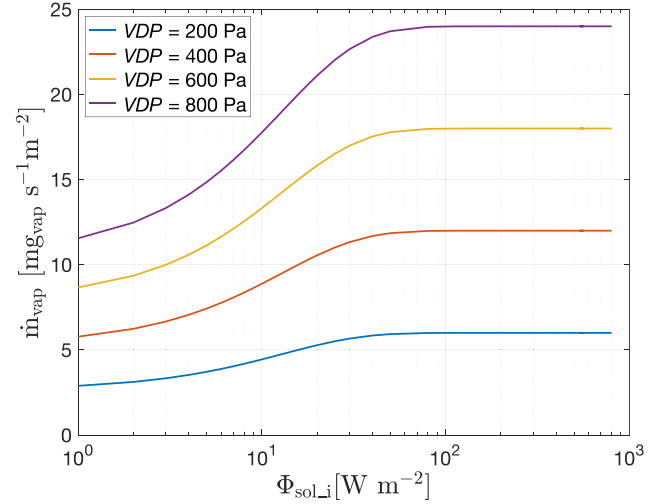| Coefficient	Value	Unit of measurement
z_1	0.154	–
z_2	1.10	–
z_3	1.13	–
z_4	1.65	W m^{-2} K^{-1}
z_5	0.56	–
z_6	13.0	W m^{-2}

Fig. 3. Evapotranspiration rates ($\dot{m}_{\text{vap}}$) calculated as a function of the solar radiation on the canopies ($\phi_{\text{sol\_i}}$) and the water Vapour Pressure Deficit (*VPD*) according to Eq. (5) (*x*-axis is in logarithmic scale).

performed considering *LAI* equal to 3 m^2 m^{-2} and four different values of *VPD*. The results show that in presence of high $\phi_{\text{sol\_i}}$ (above 100 W m^{-2}), $\dot{m}_{\text{vap}}$ is affected mainly by *VPD*, while in presence of low $\phi_{\text{sol\_i}}$, $\dot{m}_{\text{vap}}$ is mostly affected by the same solar radiation.

The term $\dot{m}_{\text{vap,j}}$ estimates the amount of water vapour that the plants transpire to the surrounding air per unit of cultivated floor area at the *j*-th time step. Knowing $\dot{m}_{\text{vap,j}}$, the equivalent latent heat load ($\phi_{\text{lat\_i,j}}$) can be estimated as

$$\phi_{\text{lat\_i,j}} = \frac{A_{\text{gh}} \cdot \dot{m}_{\text{vap,j}} \cdot \lambda}{10^3} \quad \text{[W]} \tag{6}$$

The plant transpiration converts a share of the solar radiation (sensible heat) that has entered the greenhouse ($\phi_{\text{sol\_i,j}}$) in latent heat. The remaining solar sensible heat gain ($\phi_{\text{sens\_i,j}}$) can be calculated at each time-step *j* as

$$\phi_{\text{sens\_i,j}} = \phi_{\text{sol\_i,j}} - \phi_{\text{lat\_i,j}} \quad \text{[W]} \tag{7}$$

The calculated values of $\phi_{\text{sens\_i,j}}$ and $\dot{m}_{\text{vap}}$ are inputs data for the thermal and the moisture balance solution modules, respectively.

3.3.4. Thermal balance module

The thermal balance module represents the core of the model and it is used at each simulation stage in which $\theta_{\text{air\_i}}$ has to be estimated. The thermal balance integrated in this simulation model is a customization of the simple hourly method of ISO 13790 standard [67]. The method consists in the thermal-electrical analogy between the analysed building and a resistance–capacitance (R −C) electrical network characterised by five resistances and one capacitance (5R1C), as showed in Fig. 4. In the thermal analogy, the resistances represent the heat transfer resistances, and the capacitor represents the entire building fabric heat capacity. The
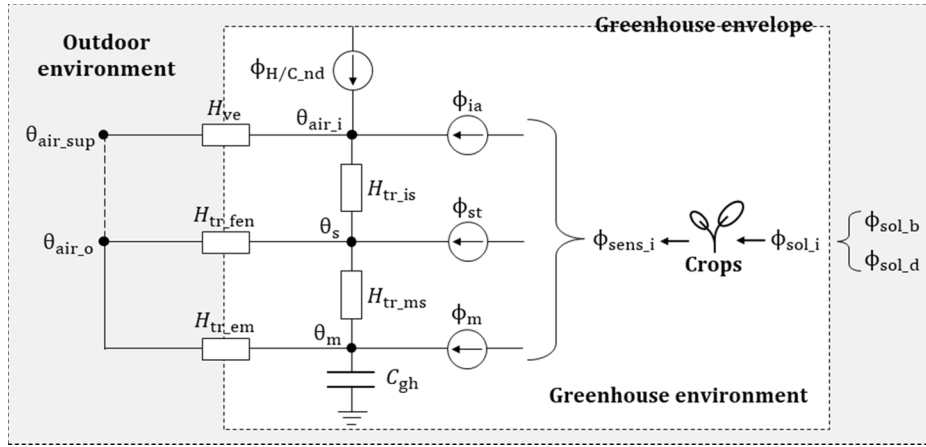
Fig. 4. Analogy between the 5R1C electrical network and the thermal behaviour of a greenhouse.

simple hourly method embeds the advantage of adopting an hourly time-step for the simulation, that is adequate to follow the variation of both solar radiation and ventilation flow rate that are typical of greenhouses. This simulation method is considered reliable by many previous studies especially focused on civil buildings [68,69]. Costantino et al. [70] applied the simple hourly method of ISO 13790 standard to agricultural buildings, comparing it with a detailed dynamic energy simulation method for estimating the energy consumption for climate control and the indoor environmental conditions of livestock houses. Then, Costantino et al. [56] developed an *ad-hoc* energy simulation model for broiler houses.

As shown in Fig. 4 (where a schematization of the present energy simulation method is presented), the supply air temperature θ_{air_sup} and the outdoor air temperature θ_{air_o} are connected to the node θ_{air_i} through the heat transfer coefficient H_{ve}, meaning that ventilation can be carried out considering θ_{air_o} or θ_{air_sup}. Supply air temperature θ_{air_sup} is considered when evaporative pads are activated, and it is the temperature of the air exiting the pads after the adiabatic saturation. The supplemental heat load ϕ_{H/C_nd} is directly applied on the node θ_{air_i}. This configuration of the thermal network entails that ϕ_{H/C_nd} and the ventilation thermal load directly affects the value of θ_{air_i} without any time delay.

The heat conduction through glazed surfaces has the same effect (no time delay) on θ_{air_i}, since the θ_{air_o} node is linked to the θ_{air_i} through the heat transfers coefficients H_{tr_fen} and H_{tr_is}. The heat transfer coefficient H_{tr_fen} represents the heat conduction across the glazed surfaces while H_{tr_is} represents the natural convection between the glazed surface and the indoor air. Conversely, the heat conduction through the opaque envelope (quite negligible in greenhouses) involves the phenomenon of heat storage and release. For this reason, the total building fabric heat capacity of the greenhouse (C_{gh}) is placed between the heat transfer coefficients H_{tr_em} and H_{tr_ms}. The heat transfer coefficient H_{tr_em} considers the heat conduction occurring from the external environment to the building thermal mass. The H_{tr_ms} considers the heat transfer between the building thermal mass and the building surface, characterised by θ_s that averages the temperature of the glazed and opaque envelope.

The developed model considers that only a fraction of the outdoor beam and diffuse solar radiation (ϕ_{sol_b} and ϕ_{sol_d}) enters inside the greenhouse (ϕ_{sol_i}). Once entered in the greenhouse enclosure, ϕ_{sol_i} is in part converted by the plants into latent heat (ϕ_{lat_i}), while the remaining sensible part (ϕ_{sens_i}) is considered in the thermal balance. A visible in Fig. 4, ϕ_{sens_i} is split into three additional heat flows, namely:

- ϕ_{ia}: convective heat flow directly applied to θ_{air_i};
- ϕ_{st}: radiative heat flow directly applied to θ_s;

- ϕ_{im}: radiative heat flow directly applied to θ_m (building mass temperature) and subjected to a time delay.

In the developed simulation model, the simple hourly method is applicated for estimating the supplemental heating/cooling theoretical thermal load ϕ_{H/C_nd} to reach the fixed set point temperatures. If neither supplemental heating nor cooling is needed (free-floating conditions), the solution of the energy balance provides θ_{air_i}.

The main equations adopted for solving the energy balance set in this calculation module are reported in Appendix A, while the complete set of equations can be found in paragraph C.3 of Annex C of ISO 13790 [67].

3.3.5. Moisture balance module

In this module, the indoor air water content (or humidity ratio) x_{air_i} is studied through the following mass balance ordinary differential equation that describes the water vapor balance inside the greenhouse in non-steady state conditions

$$\frac{dx_{air\_i}}{d\tau}\cdot V_{gh}\cdot\rho_{air} = \dot{m}_{vap}\cdot A_{gh}\cdot10^3 + \frac{\dot{V}_{air}\cdot\rho_{air}\cdot(x_{air\_sup} - x_{air\_i})}{3.6\cdot10^3} \quad \left[\frac{g_{vap}}{s}\right] \quad (8)$$

where $\frac{dx_{air\_i}}{d\tau}$ represents the variation rate of x_{air_i} (g_{vap} kg_{air}^{-1}) in time τ (s), V_{gh} is the greenhouse net volume (m³) and ρ_{air} is the volumetric mass density of air (kg m⁻³). The term $\dot{m}_{vap}$ is the transpiration water vapour flow (mg$_{vap}$ m⁻² s⁻¹), A_{gh} the greenhouse floor area (m²), $\dot{V}_{air}$ is the ventilation flow rate (m³ h⁻¹) and x_{air_sup} is the humidity ratio of the supply air (g_{vap} kg_{air}^{-1}).

The solution of the ordinary differential Eq. (8) is

$$x_{air.i}(\tau+\Delta\tau) = x_{sup} + \frac{\dot{m}_{vap}\cdot A_{gh}}{n_{ach}\cdot V_{gh}\cdot\rho_{air}}\cdot3.6\cdot10^6$$

$$+ \left[x_{air.i}(\tau) - x_{air.sup} - \frac{\dot{m}_{vap}\cdot A_{gh}}{n_{ach}\cdot V_{gh}\cdot\rho_{air}}\cdot3.6\cdot10^6\right]\cdot e^{-\left(\frac{n_{ach}}{3600\cdot\omega}\right)\cdot\Delta\tau} \left[\frac{g_{vap}}{kg_{air}}\right]$$

$$(9)$$

where $\Delta\tau$ is the time-step of simulation and n_{ach} is the number of ventilation air exchanges per hour (h⁻¹). The term ω is a dimensionless multiplier that is introduced to lump the effect of water vapour sorption and storage of the greenhouse elements in the air node.

For each simulation time-step, x_{air_i} is estimated through Eq. (9), while RH_i is obtained through a psychrometric equation from x_{air_i} and θ_{air_i}.

3.3.6. Heating system module

This calculation module estimates the thermal energy consumption

needed to maintain $\theta_{\text{set\_H}}$ in the analysed greenhouse (E_{th}) as

$$E_{\text{th}} = \frac{\sum_{j=1}^{n_{\text{sim}}} (\phi_{\text{H\_nd,j}} \cdot \Delta\tau)}{\eta_{\text{H}} \cdot 10^3} \quad [\text{kWh}] \tag{10}$$

The value of E_{th} is calculated considering $\phi_{\text{H\_nd,j}}$ (the needed thermal load at j-th time-step), the duration of the j-th time-step $\Delta\tau$ (one hour) and considering the global efficiency of the heating system η_{H} (a preliminary model input). n_{sim} is the number of the simulation time-steps.

3.3.7. Cooling pad efficiency module

This calculation module estimates the supply air temperature exiting from the evaporative pads. The direct saturation effectiveness of the evaporative pad (ε) indicates the extent to which the complete saturation of the inletting air is approached [71] and is influenced by various parameters, mainly:

- pad model: this affects ε since the air path through the pad is different according to its geometrical features, such as the pad depth and flute angle. Flute angles can be defined as the angle between the pad flutes (in which the air flows through the pads) and the vertical axis of the same pad. For example, a flute angle of 0° means that the flute is horizontal. Cellulose pads are made by vertical array of flutes with alternate angles (e.g. 30°/60° or 45°/15°).
- airspeed across the pad: low airspeeds entail high ε.

Fig. 5 (Authors elaboration on [72,73]) shows the variation of ε for different cellulose pad models as a function of the air velocity across them. The considered models differ for the thickness (100 mm and 150 mm) and for the flute angles that are 30°/60° for model 1 and 2, while they are 45°/15° for models 3 and 4. The graph shows that ε decreases considerably as a function of the air speed across the pads while it increases in thicker pads and in presence of higher flute angles (30°/60°).

In the calculation model, the user selects the pad model and, at each time-step, ε is calculated as a function of the airspeed across the pads that is estimated as the ratio between the total ventilation air flow rate and the pad area.

The calculation model activates the evaporative cooling only in the time-steps in which $\theta_{\text{air\_o}}$ is higher than $\theta_{\text{set\_C}}$. At each time-step, the supply air temperature $\theta_{\text{air\_sup,j}}$ is thus calculated as

$$\theta_{\text{air\_sup,j}} = \begin{cases} \theta_{\text{air\_o\_db,j}} - \varepsilon \cdot (\theta_{\text{air\_o\_db,j}} - \theta_{\text{air\_o,j}}) & \text{if} \quad \theta_{\text{air\_sup,j}} > \theta_{\text{set\_C}} \\ \theta_{\text{air\_o\_db,j}} & \text{if} \quad \theta_{\text{air\_sup,j}} \leq \theta_{\text{set\_C}} \end{cases} \tag{11}$$
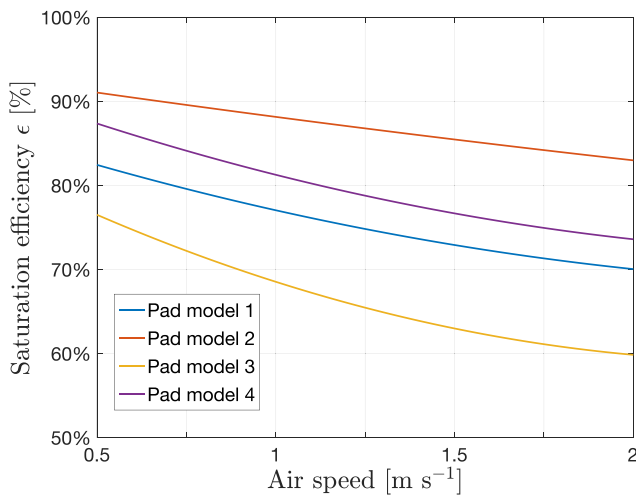

Fig. 5. Variation of the evaporative pad saturation efficiency ε of different pad models as a function of the air velocity across them. The considered pad models are characterised by different thickness (100 and 150 mm) and different flute angles (30°/60° and 15°/45°). Authors elaboration on [72,73].

where $\theta_{\text{air\_o\_db}}$ and $\theta_{\text{air\_o\_wb}}$ are the dry-bulb and the wet-bulb temperatures of the outdoor air, respectively. Please note that, even if the evaporative cooling is not activated, the inletting air crosses the pads to enter inside the greenhouse, therefore the pressure drop due to the pad presence should be always considered.

3.3.8. Dehumidification ventilation system module

In mechanically ventilated greenhouses, two main configurations of the ventilation system can be adopted. The first configuration relies in two different sets of fans, one for dehumidification and the other for cooling ventilation. This choice is since dehumidification usually needs lower ventilation flow rates than cooling ventilation, hence smaller fans can be installed. In the second configuration, a single set of fans deals with both dehumidification and cooling ventilation.

The calculations for estimating the ventilation flow rate and electrical energy consumption for dehumidification and cooling ventilation are presented in this section and in the following one. This division is since, even though the process is quite similar, these calculations are characterised by a main difference. When dehumidification ventilation is activated, in fact, the greenhouse climate control system manages the inlet opening for maintaining a fixed static pressure difference between inside and outside Δp_{st}. Therefore, Δp_{st} in ventilation for dehumidification is an input data of the model. On the contrary, when cooling ventilation is activated, Δp_{st} is unknown and it has to be estimated by the model considering, for example, the pressure drop due to the evaporative pads, as described in the following section.

This calculation module simulates the control logic of dehumidification ventilation and estimates the consequent volumetric ventilation airflow rate for dehumidification ($\dot{V}_{\text{deh}}$) needed to maintain RH_{i} below the threshold value $RH_{\text{i\_max}}$ (input data). The module also estimates the electrical energy consumption resulting from the use of fans.

Depending on the values of $x_{\text{air\_sup}}$ (supply air humidity ratio) and $x_{\text{air\_i\_MAX}}$ (the maximum $x_{\text{air\_i}}$ that ensures to maintain RH_{i} below $RH_{\text{i\_max}}$), different conditions may occur as visible in Fig. 6, where the ventilation logic implemented in the model is schematized. According to that diagram, three different situations can occur at each simulation time step depending on the value of $x_{\text{air\_sup}}$. The first situation (A) is typical of a winter day with $x_{\text{air\_sup}}$ lower than $x_{\text{air\_i\_MAX}}$. In this situation, the outdoor supply air can be used to maintain $RH_{\text{i\_max}}$. In this situation, the ventilation airflow rate for dehumidification ($\dot{V}_{\text{deh}}$) is calculated as

$$\dot{V}_{\text{deh}} = min \left[\frac{\dot{m}_{\text{vap}} \cdot A_{\text{gh}} \cdot 3.6}{\rho_{\text{air}} \cdot (x_{\text{air\_i\_MAX}} - x_{\text{air\_sup}})}; \dot{V}_{\text{inst}} \right] \quad \left[\frac{\text{m}^3}{\text{h}} \right] \tag{12}$$

where $x_{\text{air\_sup}}$ is the humidity ratio of the supply air and $x_{\text{air\_i\_MAX}}$ is the maximum value of $x_{\text{air\_i}}$ that ensures to maintain RH_{i} below $RH_{\text{i\_max}}$ (both expressed in $\text{g}_{\text{vap}} \text{ kg}_{\text{air}}^{-1}$). $\dot{V}_{\text{inst}}$ represents the maximum ventilation capacity (for dehumidification) installed in the greenhouse and it is considered because $\dot{V}_{\text{deh}}$ can never be higher than $\dot{V}_{\text{inst}}$. The value of $x_{\text{air\_i\_MAX}}$ (needed in Eq. (12)) is calculated using the following psychrometric equation

$$x_{\text{air\_i\_MAX}} = 0.622 \cdot \frac{RH_{\text{i\_MAX}} \cdot p_{\text{vs}}(\theta_{\text{air\_i}})}{p_{\text{atm}} - RH_{\text{i\_MAX}} \cdot p_{\text{vs}}(\theta_{\text{air\_i}})} \quad \left[\frac{\text{g}_{\text{vap}}}{\text{kg}_{\text{air}}} \right] \tag{13}$$

where $p_{\text{vs}}(\theta_{\text{air\_i}})$ is water saturated vapour pressure at $\theta_{\text{air\_i}}$ and p_{atm} is the atmospheric pressure (in Pa). In the time-steps in which $\theta_{\text{air\_i}}$ is not know (free-floating conditions), the value of $x_{\text{air\_i\_MAX}}$ cannot be calculated directly through Eq. (13) and the model performs an iterative procedure up to convergence. This iterative procedure consists in the application of the thermal balance module using the output value of $\theta_{\text{air\_i}}$ to estimate the $x_{\text{air\_i\_MAX}}$ using Eq. (13). Once $x_{\text{air\_i\_MAX}}$ is known, the module re-applies Eq. (12) and (13) in loop until the convergence.

The second situation presented in Fig. 6 (B) is common in autumn, spring, and summer. Since $x_{\text{air\_sup}}$ and $x_{\text{air\_i\_MAX}}$ are very close between
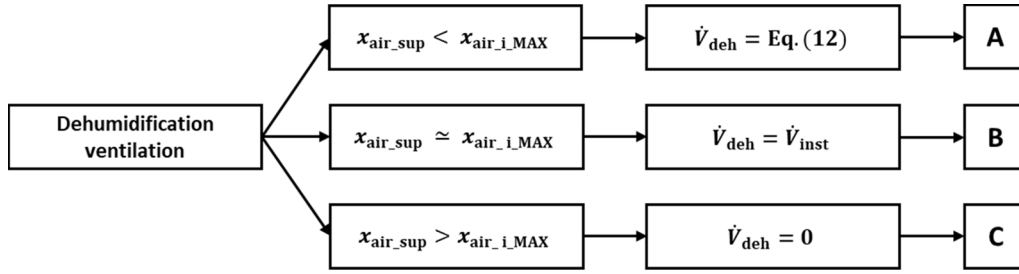
Fig. 6. Control logic for the dehumidification ventilation adopted in the present model.

them, a high dehumidification ventilation flow rate is needed. For this reason, the maximum ventilation capacity for dehumidification installed in the greenhouse ($\dot{V}_{\text{inst}}$, commonly a 5–6 ach) is provided. The last situation (C) may also happen during autumn, spring, and summer (like the previous conditions). When $x_{\text{air\_sup}}$ is higher than $x_{\text{air\_i\_MAX}}$, ventilation cannot reduce RH_i (as visible from Eq. (12)) and the only way to decrease the RH_i is by increasing $\theta_{\text{air\_i}}$. This strategy is suitable during autumn and spring, but it increases the greenhouse thermal energy consumption, and its adoption is led by economic considerations. During summer, the increase of $\theta_{\text{air\_i}}$ to reduce RH_i is not adopted since it has the opposite effect of cooling ventilation.

The presented energy model was developed to simulate greenhouses equipped with fixed and/or variable angular speed fans, therefore the greenhouses can be simulated considering two sets of fans that carry out, respectively, dehumidification and cooling ventilation, or a single set that deals with both the tasks. Fixed angular speed fans cannot control the propeller speed and they provide a single value of airflow as function only of the fan operative static pressure Δp_{st}, that is the difference between the pressure that would be measured upstream and downstream of the fan (inside and outside the greenhouse). To obtain the desired ventilation rate, fixed angular speed fans are operated according to a duty cycle (intermittent activation). On the contrary, variable angular speed fans can modulate the propeller speed for providing exactly the needed ventilation rate.

This difference should be considered when fans are modelled. In particular, the ventilation flow rate $\dot{V}_{\text{fan\_fix}}$ for a fixed angular speed fan reads

$$\dot{V}_{\text{fan\_fix}} = a_{\text{flow}} \cdot \Delta p_{\text{st}}^2 + b_{\text{flow}} \cdot \Delta p_{\text{st}} + c_{\text{flow}} \quad \left[\frac{\text{m}^3}{\text{h}}\right] \tag{14}$$

where a, b and c are interpolation parameters for ventilation rate (subscript *flow*).

To estimate the electrical energy consumption for ventilation E_{el}, the Specific Fan Performance (*SFP*) is considered. The *SFP* represents the hourly flowrate delivered by the fan per each watthour of electrical energy consumption. For a fixed angular speed fan, the *SFP* reads

$$SFP_{\text{fix}} = a_{\text{perf}} \cdot \Delta p_{\text{st}}^2 + b_{\text{perf}} \cdot \Delta p_{\text{st}} + c_{\text{perf}} \quad \left[\frac{\text{m}^3}{\text{Wh}}\right] \tag{15}$$

where a, b and c are interpolation parameters for *SFP* (subscript *perf*).

Eq. (14) and (15) show that for fixed angular speed fans, both the flowrate and the *SFP* vary only on a single curve as a function of Δp_{st} only, as shown in Fig. 7. As stated before, in dehumidification ventilation, Δp_{st} is known since the automatic climate control system of the greenhouse maintains Δp_{st} constant at the established value (usually 20 Pa) by opening and closing the fan shutters and the greenhouse openings. In the simulation model, the user can set the value of Δp_{st} that has to be maintained by the dehumidification ventilation.

Conversely, a variable angular speed fan operates with a set of operative curves depending on the propeller speed and, thus, both the flowrate and the *SFP* (at the same value of Δp_{st}) can get different values depending on the propeller speed, as shown in Fig. 8. The graph shows that when a variable angular speed fan is operated at a low propeller speed (such as 60% of the maximum speed), the flowrate (Fig. 8a) is lower if compared with high propeller speeds (such as 100% of the maximum speed), but the specific performance (Fig. 8b) increases considerably (at the same Δp_{st}) and less energy is needed by the fan to deliver the same amount of air. For this reason, climate control systems of greenhouses usually share the ventilation flow rate between the installed fans with the aim of making them work at low angular speeds (usually around 60–70% of the maximum speed). Higher angular speeds are reached only when high ventilation flow rates are needed.

The estimation of the propeller speed needed to ensure the required flowrate is not an easy task and, consequently, the calculation of the *SFP*
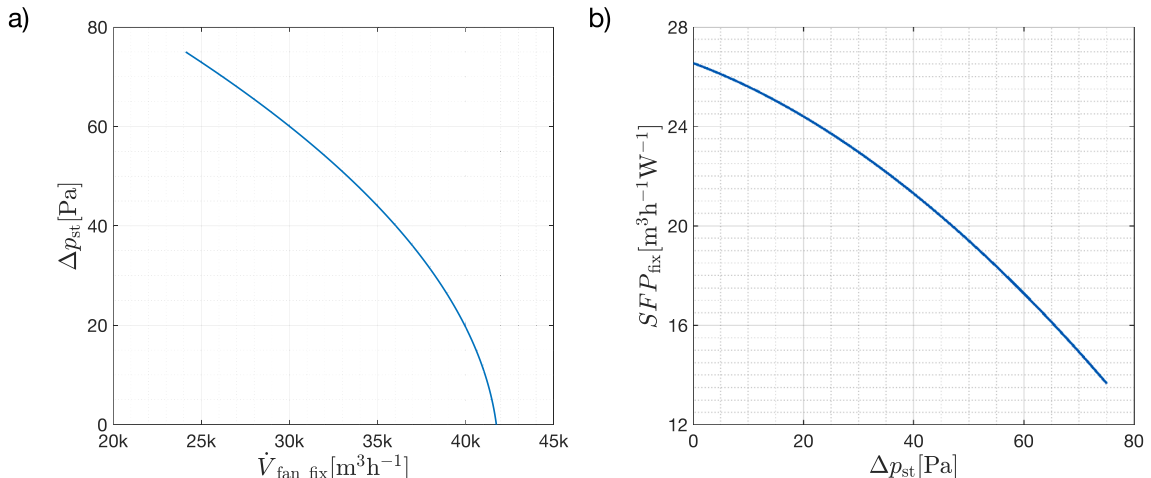

Fig. 7. Fixed speed fan (a) flowrate and (b) Specific Fan Performance (SFP) as function of fan static pressure.
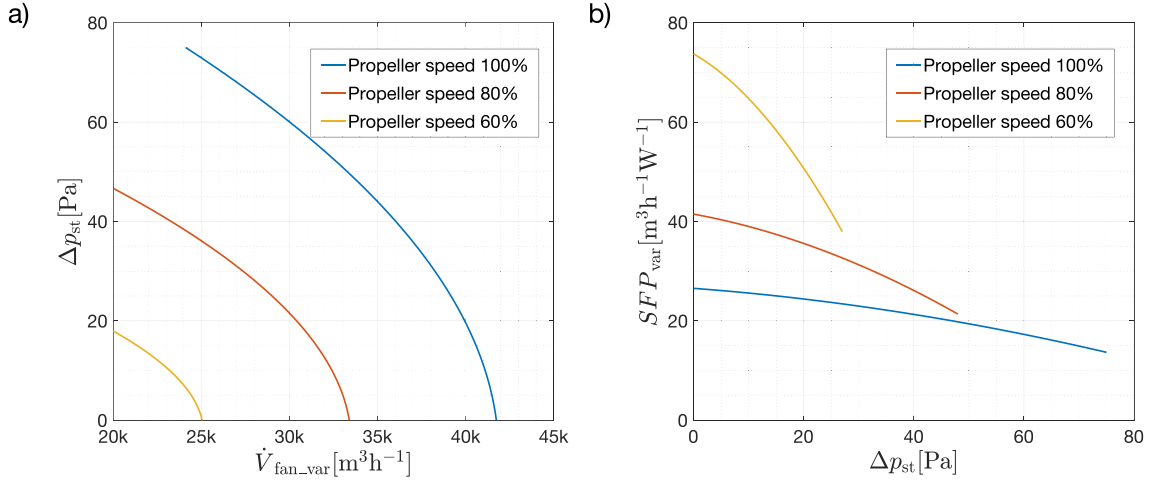
a)

b)

Fig. 8. Variable speed fan (a) flowrate and (b) Specific Fan Performance (*SFP*) as function of static pressure.

of a variable angular speed fan is more complex than for a fixed angular speed fan. The solution for calculating the *SFP* consists in generating a set of additional fictitious variables defined as a combination of the flowrate $\dot{V}_{\text{fan\_var}}$ and Δp_{st} to interpolate the energy consumption of the fan at different propeller speed. An example of that a process is

$$SFP_{\text{var}} = d_{\text{perf}} \cdot \dot{V}_{\text{fan\_var}} + e_{\text{perf}} \cdot \dot{V}_{\text{fan\_var}}^2 + f_{\text{perf}} \cdot \Delta p_{\text{st}} + g_{\text{perf}} \cdot \Delta p_{\text{st}}^2$$
$$+ h_{\text{perf}} \cdot \Delta p_{\text{st}} \cdot \dot{V}_{\text{fan\_var}} + i_{\text{perf}} \quad \left[\frac{\text{m}^3}{\text{Wh}}\right] \tag{16}$$

where $d_{\text{perf}}, e_{\text{perf}}, f_{\text{perf}}, g_{\text{perf}}, h_{\text{perf}}$ are interpolation coefficients that depend on the model of variable speed fans. In this case, $\dot{V}_{\text{fan\_var}}$ has the same value of $\dot{V}_{\text{deh}}$ since this fan type provides exactly the required ventilation flow rate.

Knowing the *SFP* of both fixed and variable angular speed fans, the electrical energy consumption for dehumidification ventilation $E_{\text{el\_deh}}$ is calculated as

$$E_{\text{el\_deh}} = \sum_{i=1}^{n_{\text{fan}}} \left(\frac{SFP_{\text{fix/var,z}} \cdot \dot{V}_{\text{fan\_fix/var,z}}}{10^3} \right) \quad [\text{kWh}] \tag{17}$$

where $SFP_{\text{fix/var,z}}$ and $\dot{V}_{\text{fan\_fix/var,z}}$ are the *SFP* and the ventilation flow rate of the *i*-th fixed or variable angular speed fan. The term n_{fan} indicates number of fans that are present in the ventilation system.

3.3.9. Cooling ventilation system module

This calculation module simulates the control logic of the cooling ventilation and estimates the ventilation air flow rate needed to maintain the required $\theta_{\text{air\_i}}$ and the resulting electrical energy consumption. The previously obtained value of $\phi_{\text{C\_nd}}$ (sensible cooling load) is used to calculate the hourly ventilation rate needed for cooling $\dot{V}_{\text{cool}}$.

The cooling ventilation logic implemented in this model as schematized in Fig. 9. Two different types of control can be performed inside greenhouses. The first type of control is the temperature control, and it maintains a fixed $\theta_{\text{set\_C}}$ in a certain spot of the greenhouse (where the climate control probe is placed). When temperature control is performed, two different situations can occur depending on $\theta_{\text{air\_sup}}$. If $\theta_{\text{air\_sup}}$ is lower than $\theta_{\text{set\_C}}, \dot{V}_{\text{cool}}$ (situation A of Fig. 9) is calculated from $\phi_{\text{C\_nd}}$ as

$$\dot{V}_{\text{cool}} = min\left[\frac{\phi_{\text{C\_nd}} \cdot 3.6 \cdot 10^3}{\rho_{\text{air}} \cdot c_{\text{air}} \cdot \left(\theta_{\text{air\_i}} - \theta_{\text{air\_sup}}\right)}; \dot{V}_{\text{inst}}\right] \quad \left[\frac{\text{m}^3}{\text{h}}\right] \tag{18}$$

where c_{air} is the specific heat capacity of the air (in $\text{J kg}^{-1}\text{ K}^{-1}$) and ρ_{air} its
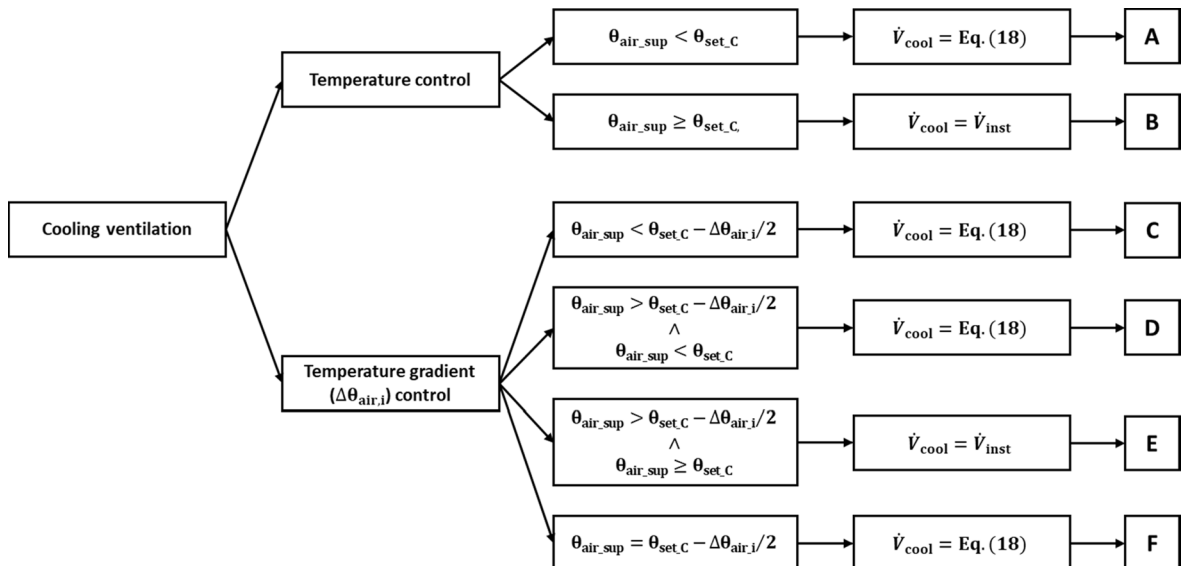

Fig. 9. Control logic for the cooling ventilation adopted in the present model.

volumetric mass density (kg m^{-3}). The term $\dot{V}_{\text{inst}}$ represents the maximum ventilation capacity (for cooling) actually installed in the greenhouse. This term is considered in Eq. (18) since $\dot{V}_{\text{cool}}$ can never be higher than $\dot{V}_{\text{inst}}$. If $\theta_{\text{air\_sup}}$ is higher than $\theta_{\text{set\_C}}$, $\theta_{\text{set\_C}}$ cannot be maintained and $\dot{V}_{\text{inst}}$ is provided (situation B of Fig. 9).

The second type of temperature control maintains a minimum fixed value of temperature gradient ($\Delta\theta_{\text{air\_i}}$, of 3–4 °C) between two spots of the greenhouse (usually the beginning and the end) in addition to guarantee $\theta_{\text{set\_C}}$. This temperature control criterion is adopted to prevent the crop from being subject to different temperatures and, thus, different growing conditions depending on their position in the greenhouse. In the first situation of temperature gradient control presented in Fig. 9 (situation C), $\theta_{\text{air\_sup}}$ is smaller than the set point gradient, therefore $\dot{V}_{\text{cool}}$ can decrease $\theta_{\text{air\_i}}$. In the second situation (D), $\Delta\theta_{\text{air\_i}}$ (an input data of the model and of the greenhouse climate control system) should be reduced to make it possible to guarantee $\theta_{\text{set\_C}}$. The third situation (E) is the worst one since outdoor air cannot be used to achieve $\Delta\theta_{\text{air\_i}}$. In this situation, the maximum cooling ventilation capacity $\dot{V}_{\text{inst}}$ is used or evaporative cooling is activated. Last situation (F) is the one in which $\theta_{\text{air\_sup}}$ has the same value of the $\theta_{\text{set\_C}}$ considering also $\Delta\theta_{\text{air\_i}}$. Please note that, when it is present, evaporative cooling can be activated in each one of situations presented in Fig. 9. Its activation, in fact, reduces $\theta_{\text{air\_sup}}$ and, consequently, also $\dot{V}_{\text{cool}}$ and $E_{\text{el\_deh}}$.

In the calculation of the electrical energy consumption for cooling ventilation $E_{\text{el\_cool}}$, the main difference with respect of the dehumidification ventilation calculation (as stated before) is that in cooling ventilation Δp_{st} is unknow, since is not maintained constant by the climate control system but depends on the air speed through the pads and, consequently by the ventilation rate.

To estimate Δp_{st}, the pressure drop due to the presence of evaporative pads is considered. Inlet air, in fact, enters through the pads, even when they are not activated. The static pressure that is generated by the air flow passing through the cooling pad system (15–20 Pa at maximum airflow) can be estimated by the data provided by the manufacturers of the pads that express the static pressure drop as a function of the air velocity across the pad, as reported in Fig. 10 (Authors elaboration on [72,73]), where the same pad models of Fig. 5 are presented. The graph shows that pad models with higher flute angles (i.e. 30°/60°) are responsible of higher static pressure drops.

The pressure drop due to pads presence is the main component for the calculation of Δp_{st} since the distributed static pressure drop due to the airflow crossing the greenhouse can be neglected. The low airspeed

inside the greenhouse (usually does not overcome 0.75 m s^{-1}), in fact, entails negligible values of pressure drops around 1 or 2 Pa.

To calculate $E_{\text{el\_cool}}$, two different approaches are followed by the model depending on the type of fan used. For cooling purposes, in fact, both fixed and variable angular speed fans can be used, similarly to what happens for dehumidification ventilation.

When fixed angular speed fans are used, the aeraulic circuit resistance curve (pad curve of Figure) and the fans performances curves of Fig. 7 are crossed to estimate the ventilation flowrate generated by the fixed angular speed fans during cooling ventilation (solution of a system of two equations in two variables). Fig. 11 represents the approach followed by the calculation model to estimate the ventilation capacity of the system according to the number of fans that are activated. A higher number of fans means a higher ventilation rate but also a higher Δp_{st} and, thus, a lower ventilation capacity of each fan.

Once the ventilation capacity of the system is calculated, $E_{\text{el\_cool}}$ is estimated knowing Δp_{st} using the *SPF*, with an equation similar to Eq. (17).

When variable speed fans are used, the calculation is simpler since the ventilation provided by fans is exactly $\dot{V}_{\text{cool}}$ calculated through Eq. (18) as fans can modulate their propeller speed. In addition, also the static pressure is easily calculated since it consists in applying the pad curve equation with the airspeed resulting from the $\dot{V}_{\text{cool}}$ flowrate. *SFP* and $E_{\text{el\_cool}}$ are calculated in a similar way to the dehumidification ventilation, referring to Eq. (16) and (17).

Finally, the overall electrical energy consumption E_{el} for ventilation (dehumidification and cooling) is calculated as

$$E_{\text{el}} = \sum_{j=1}^{n}\left(E_{\text{el\_deh,j}} + E_{\text{el\_cool,j}}\right) \quad [\text{kWh}] \tag{19}$$

where $E_{\text{el\_deh,j}}$ and $E_{\text{el\_cool,j}}$ are the electrical energy consumption for dehumidification and cooling at the *j*-th time-step, respectively and *n* is the number of the time-steps of the simulation period.

4. Model calibration and validation

4.1. Calibration and validation overview

The presented energy simulation model is validated against real monitored data for guaranteeing the reliability of the results. Before the validation, a calibration process is carried out. This step is needed because mathematical models for predicting greenhouse climate conditions need a calibration of their parameters before their validation
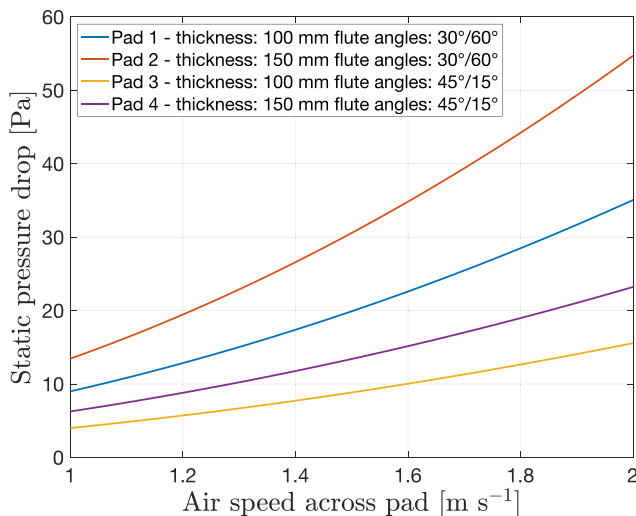

Fig. 10. Static pressure drop generated by the cooling pad according to the model and thickness. Authors elaboration on [72,73].
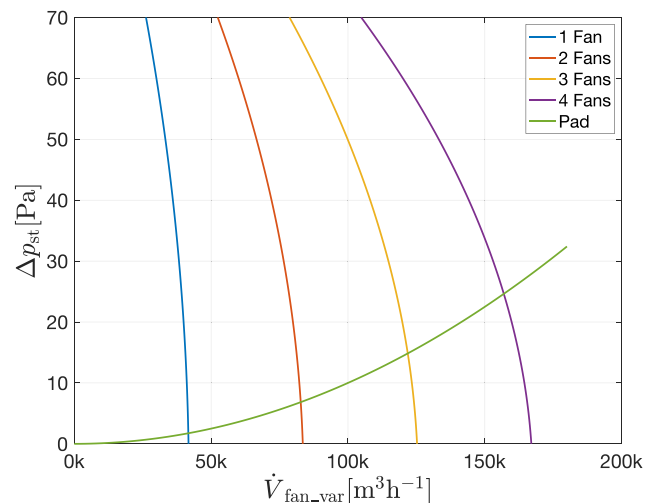

Fig. 11. Ventilation system performance, the fan operative condition is correlated to the type of cooling pad.

[74]. This is especially true in first principles models because they rely on physical equations based on several parameters (e.g. $U-value$ and greenhouse thermal capacity) that could be difficult to adjust [47]. Calibration process alters the model parameters making them more similar to the ones of the physical world and obtaining a better fit between simulated and measured data [75].

In the framework of this work, a dataset of indoor air temperature θ_{air_i}, relative humidity RH_i and electrical energy consumption E_{el} was acquired from a selected case study. Part of those data were used to perform an optimization-based calibration [76], while the remaining part (the greatest one) was used to validate the simulation model in compliance with the main international protocols and guidelines.

4.2. Case study

4.2.1. Case study description

A multi-span greenhouse for experimental cultivations located in Northeast Italy was selected as a suitable case study site. The considered building, which is part of a larger greenhouse complex for floricultural production, was favourably chosen due to its layout, its management, and the installed heating and cooling equipment. Furthermore, being devoted to experimental cultivation of new hybrid plants (small flowers), its indoor climate is accurately controlled to provide the adequate conditions to the sensitive new cuttings.

The schematic layout and the main geometrical dimensions of the monitored case study are presented in Fig. 12. As shown by the figure, the greenhouse is composed by seven bays (6.4 m of width each one) with a metal frame structure and a single glazing envelope. Part of the envelope is white painted to reduce the solar radiation gains. The main axis of the bays is aligned with northwest-southeast direction and the southwest wall is considered adiabatic since in direct contact with a conditioned space. The useful floor area is approximately 1690 m^2 while the enclosed volume is around 7510 m^3 and, inside, the cultivation is carried out on benches. Inside the greenhouses, insect proof screens are adopted to reduce the pest population and to entail a lower incidence of insect-transmitted diseases [77]. These screens lead to a further pressure drop to be considered when ventilation flow rate and SFP are calculated. The increase of pressure drop is calculated according the equation reported in [78].

The production cycle takes 60 days to be completed and, according to the greenhouse technicians, the LAI at the beginning of the production cycle can be estimated around 0.4 m^2 m^{-2}, while at the end it increases up to 1.6 m^2 m^{-2}. In the simulation model, the LAI variation in time is approximated with a linear behaviour.

The thermophysical properties of the envelope were estimated for both the glazed surfaces and the floor. The $U-value$ of the single glazed envelope (including the metal frame) is equal to 6.3 W m^{-2} K^{-1} as re-

ported in [25,79], while the internal areal heat capacity is considered negligible due to its due to its minor relevance. The floor is a concrete slab (0.2 m of thickness) and its $U-value$ was estimated to be 3.7 W m^{-2} K^{-1}, while its internal areal heat capacity is 181.2 kJ m^{-2} K^{-1}.

To calculate the total heat capacity of the greenhouse, the heat storage property of the main elements contained inside the greenhouse (e.g. soil and cultivation benches) are considered. Table 2 shows the heat capacity of the different elements considered for this calculation. The total heat capacity of the greenhouse (C_{gh}) is estimated to be 476,957 kJ K^{-1}. Nevertheless, C_{gh} is characterised by a great uncertainty since the estimation of the total amount of the elements present inside the greenhouse, their volumetric mass density and their specific heat value is a complex task. For this reason, a calibration parameter will be applied to C_{gh}, as shown later in the text.

The heating system of the greenhouse is centralized, and a gas boiler (460 kW of heating capacity) produces the supplemental heat that is transferred and distributed into the enclosure through a hydronic pipe system hanging above the cultivation benches. The climate control system guarantees θ_{set_H} of 16 °C during daytime and 14° C during nighttime (a sort of setback temperature).

In the greenhouse, an exhaust ventilation system deals with both dehumidification and cooling ventilation. The dehumidification ventilation is carried out to maintain a RH_{air_max} of 65%, while cooling ventilation is activated to maintain θ_{set_C} of 27.7° C and a maximum temperature gradient of 0.6 °C. The ventilation air flow rate is provided by seven variable angular speed fans with a diameter of 52'' (1.32 m) that are placed on the southwest wall of the greenhouse. In free delivery conditions (Δp_{st} = 0 Pa) and at 495RPM (the optimum energy efficiency), each one of the installed cone fans can provide a ventilation flow rate of 53,200 m^3 h^{-1}. In Table 3, The coefficients to be used in Eq. (16) for calculating the SFP of the installed fan model are presented (data from technical datasheet). In the northwest wall (opposite to the one of the fans), evaporative pads are placed. The installed pads are

Table 2
Heat capacities of the greenhouse elements considered in this work.

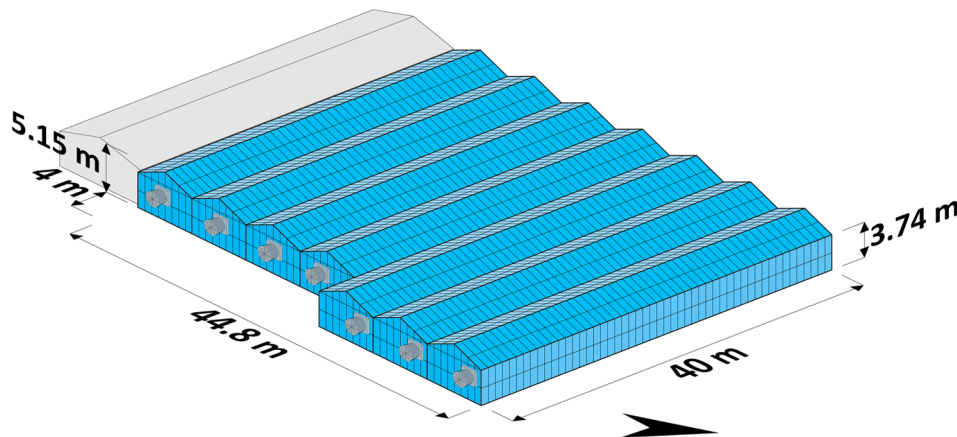| Element	Heat capacity value [kJ K^{-1}]
Greenhouse floor	147,875
Aluminium cultivation benches	14,500
Soil for plant cultivation	288,990
Water in hydronic pipe system (heating and irrigation)	15,052
Cultivated plants	1437
Air inside the enclosure	9102
Total	476,957

Fig. 12. Schematization of the monitored case study with the main geometrical dimensions.

Table 3
Performance parameters of the fan model installed in the monitored greenhouse for the SFP calculation (data from manufacturer).

Coefficient	Value	Unit of measurement
d_{perf}	$6.418 \cdot 10^{-4}$	W^{-1}
e_{perf}	$-3.382 \cdot 10^{-8}$	$h\ m^{-3}\ W^{-1}$
f_{perf}	-2.579	$m^3\ h^{-1}\ W^{-1}\ Pa^{-1}$
g_{perf}	$1.028 \cdot 10^{-2}$	$m^3\ h^{-1}\ W^{-1}\ Pa^{-2}$
h_{perf}	$2.973 \cdot 10^{-2}$	$W^{-1}\ Pa^{-1}$
i_{perf}	96.188	$m^3\ Wh^{-1}$

0.15 m thick, with flute angles of $30°/60°$, and a direct saturation effectiveness of 91% (estimated considering an air velocity across the pads of 0.5 m s^{-1}).

The monitored greenhouse is equipped with circulating fans to decrease the thermal stratification and with solar shading screens to control the incoming solar radiation. The screens are activated when the outdoor solar radiation is higher than 600 W m^{-2} or when $\theta_{\text{air\_i}}$ is higher than 26 °C. The climate control system manages the bay openings for dehumidification ventilation maintaining the required Δp_{st} fixed at 22 Pa.

4.2.2. Monitoring campaign

A monitoring campaign was carried out inside the selected case study with the aim of acquiring the needed data for calibrating and validating the developed energy simulation model. The data were acquired through an *ad-hoc* installed sensor network that monitored the indoor air temperature $\theta_{\text{air\_i}}$, the relative humidity RH_i and the electrical power absorbed by ventilation fans. The monitoring campaign concerned 360 h at the beginning of a production cycle during July 2018 (warm season).

The values of $\theta_{\text{air\_i}}$ and RH_i were collected using the following devices (accuracy noted in brackets):

- four data loggers that embed a thermistor for the measurement of $\theta_{\text{air\_i}}$ (± 0.21 °C) and a humistor for the measurement of RH_i ($\pm 2.5\%$);

- 11 resistance temperature detectors PT1000 (± 0.15 °C) connected to analog portable loggers for the measurement of $\theta_{\text{air\_i}}$ (Fig. 13 (a) and (b)).

The adopted $\theta_{\text{air\_i}}$ and RH_i sensors are characterized by high accuracies that make them suitable to be used for the objective of this work. The errors due to the sensor accuracy is considered negligible (as done in similar works present in literature [41,80]), therefore those errors are not considered in the model validation stage.

All the data loggers adopted a USB communication protocol, and all the sensors were shielded from direct solar radiation (Fig. 13 (a)). Using the previously described devices, $\theta_{\text{air\_i}}$ was monitored in 15 different spots inside the enclosure and RH_i in four different spots. The sensors were spaced inside the enclosure (e.g. in the centre, close to the pads and the fans) and at different height from the floor (0.5, 1.0, 1.5 and 2.0 m). The numerosity of the installed sensors was because greenhouses are characterised by a not homogenous indoor thermal environment and the indoor climate conditions may differ considerably between the different spots of the enclosure [81]. The acquisition time-step was set from one to ten minutes, according to the memory capacity of the different devices. The outdoor weather data were obtained from a third part weather station (Regional Agency for the Protection of the Environment of Veneto, ARPAV) near to the monitored greenhouse, that provides the values of $\theta_{\text{air\_o}}$, RH_o and total (beam and diffuse) solar radiation on horizontal plane.

The electrical power absorbed by the fans was monitored using split-core current transformers placed in the electrical panel of the greenhouse and connected to kWh transducers (Fig. 13 (c)) set with a 10-second logging time-step. The split-core current transformers have $\pm 0.75\%$ of accuracy, an error that is considered negligible for this application and, therefore, neglected for the model validation stage.

The entire dataset acquired through the monitoring campaign have been processed to be comparable with the simulation outputs obtained for the same time period. Since the developed energy simulation model is a lumped parameter one with an hourly time step, the values of $\theta_{\text{air\_i}}$ and RH_i that were monitored in the different spots of the enclosure were first spatially averaged (through the arithmetic mean) between them to obtain single values properly representative of the indoor environmental
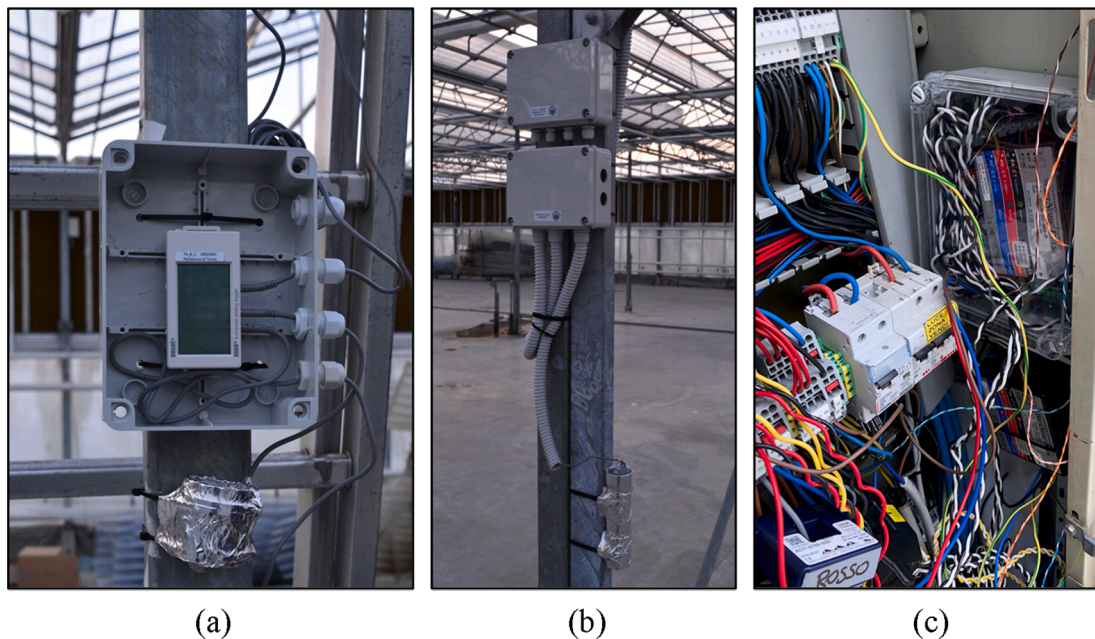

Fig. 13. (a) Analog data logger with three PT1000 temperature detectors (installation stage). (b) Analog portable data logger ready for the monitored campaign. In the bottom, the figure shows also the device adopted to shield the air temperature probe from solar radiation (c) Detail (split-core current transformer and kWh transducers) of the monitoring systems installed in the electrical panel of the greenhouse.

conditions of the entire enclosure at each logging time step. Then, the time profiles of the measured variables were temporally averaged (also through the arithmetic mean) over one hour obtaining three measured-based temporal profiles: (1) the $\widetilde{\mathscr{A}}$ set constituted by the hourly average of the measured θ_{air_i}, (2) the $\widetilde{\mathscr{B}}$ set constituted by the hourly average of the measured RH_i and the $\widetilde{\mathscr{C}}$ set constituted by the hourly values of monitored electrical energy consumption.

The $\widetilde{\mathscr{A}}$, $\widetilde{\mathscr{B}}$ and $\widetilde{\mathscr{C}}$ time profiles were thus divided into two disjoint subsets each one: the first one (72 h) is used to calibrate the model, while the second one (288 h) is used to validate it through a calibrated simulation.

4.3. Model calibration

4.3.1. Calibration parameters definition

In the present work, an optimisation-based calibration [82,83] is adopted and, for this aim, an optimisation problem is set, defining the optimisation parameters (even called calibration parameters), the objective functions and constrains of the problem. The selection of parameters to be calibrated was performed considering the aspects of the model that are characterised by a higher uncertainty, due to modelling simplifications (e.g. plant transpiration and greenhouse heat storage phenomena) or the use of literature data instead of measured ones. In addition, the adopted calibration parameters were selected on purpose among the input data (that are constant during the entire simulation) with the aim of not affecting the dynamics of any physical phenomenon.

The thermal transmittances of the glazed surfaces and of the floor, which were estimated from on-site inspections, are characterised by a high uncertainty. For this reason, the calibration parameters γ_{glass} and γ_{floor} are introduced. Both the defined parameters are dimensionless multiplicative factors of the $U-values$ of glazed surfaces and floor (constant input data), respectively.

The calibration stage also concerns the heat and moisture storage property since, as previously stated, the estimation of heat and moisture capacity is deeply affected by the properties of the elements contained inside the building that, in a complex environment such a greenhouse, are difficult to be properly determined. Since several parameters affect the preliminary assessment of heat and moisture capacity, the dimensionless calibration parameter γ_{th} and γ_{hig} are defined. The calibration parameter γ_{th} is a multiplier of C_{gh}, while γ_{hig} is a multiplier of ω presented in Eq. (9). Both the terms C_{gh} and ω are input data that are constant during the entire simulation.

Another source of uncertainty in the model is the plant *LAI* dynamics of the grown experimental cultivations, the accurate measurement of which is destructive [84] or very difficult [85]. In this work, the *LAI* variation in time was modelled with a linear function characterised by the slope m_{LAI} and the y-intercept q_{LAI}. In the calibration process, m_{LAI} and q_{LAI} are corrected by the two dimensionless multiplicative parameters γ_{m_LAI} and γ_{q_LAI}, respectively. The calibration parameter γ_{q_LAI}, therefore, modifies the *LAI* value of the plants at the beginning of the simulation, while γ_{m_LAI} calibrates the velocity of plant growth during the same simulation. The introduction of γ_{q_LAI} and γ_{m_LAI} do not affect the dynamic of the plant growth since *LAI* still changes with an hourly basis.

4.3.2. Objective functions definition

The previously defined set of calibration parameters is organized in two column vectors (Ψ and Ω) since the optimization process is performed in two consecutive steps. In the first step, the calibration parameters related to the sensible heat (vector Ψ) are optimized for minimizing the deviation between the monitored and the measured indoor air temperatures. In the second step, the set of calibration parameters mainly related with the indoor air humidity (vector Ω) are optimized for minimizing the deviation between the monitored and the measured indoor air relative humidity. Vectors Ψ and Ω read

$$\Psi = \begin{bmatrix} \gamma_{glass} \\ \gamma_{floor} \\ \gamma_{th} \end{bmatrix} \tag{20}$$

$$\Omega = \begin{bmatrix} \gamma_{m\_LAI} \\ \gamma_{q\_LAI} \\ \gamma_{hig} \end{bmatrix} \tag{21}$$

The deviation between the simulated and measured values is quantified through the Root Mean Square Error (*RMSE*) calculated between the simulated and measured values of θ_{air_i} and RH_i. The *RMSE* is defined as

$$RMSE\left(X,\widetilde{X}\right) = \sqrt{\frac{\sum_{j=1}^{n_{set}}\left(\chi_j - \widetilde{\chi}_j\right)^2}{n_{set}}} \qquad [°C] \tag{22}$$

where (X) is the vector representing the simulated time profiles and $\widetilde{X}$ the vector representing the measured ones. In Eq. (22), χ_j and $\widetilde{\chi}_j$ are the simulated and measured values, respectively, while n_{set} represents the cardinality of the considered subset (72 for the calibration phase).

During the first step of the optimization process, firstly, a Generalized Reduced Gradient (*GRG*) nonlinear algorithm is used to solve the following optimisation problem

$$\widehat{\Psi} = \min_{\Psi}\left[RMSE\left(\mathscr{A}(\Psi),\widetilde{\mathscr{A}}\right)\right] \tag{23}$$

to find the optimal set of parameter values $\widehat{\Psi}$ for θ_{air_i}. Then, in the second step, the *GRG* nonlinear algorithm was used to solve the following optimisation problem

$$\widehat{\Omega} = \min_{\Omega}\left[RMSE\left(\mathscr{B}(\Omega),\widetilde{\mathscr{B}}\right)\right] \tag{24}$$

where $\widehat{\Omega}$ is the vector of the set of the calibration parameters that minimizes the *RMSE* for RH_i, similarly to Eq. (23).

A set of constrains are fixed for the two considered optimisation problems to decrease the calculation time and to ensure to obtain results that are reliable from a physical point of view and that respect the assumptions that are presented later in the text.

The defined constrains are the following:

$$0.75 \leq \gamma_{glass} \leq 1.25 \tag{25}$$

$$0.75 \leq \gamma_{floor} \leq 1.25 \tag{26}$$

$$\gamma_{th} \geq 1 \tag{27}$$

$$\gamma_{LAI\_ang} > 0 \tag{28}$$

$$\gamma_{hig} \geq 1 \tag{29}$$

The constrains of Eq. (25) and (26) are set considering that an error by $\pm 25\%$ can be present in the estimation of the U-values from literature. The constraint for γ_{cap} (Eq. (27)) is needed since the total greenhouse heat capacity must be positive ($\gamma_{cap} > 0$) and because its first estimation was precautionary, therefore it is assumed that a lower value is very improbable ($\gamma_{cap} \geq 1$). The constrain related to *LAI* calibration parameter (γ_{LAI_ang}) is needed since the *LAI* value should increase as a function of time and the function should be bijective (Eq. (28)). No constrains were defined for γ_{q_LAI}. The constrain of the calibration parameter γ_{hig} is set to have a value higher than one (Eq. (29)) since the first approximation of the hygric capacity of the greenhouse only considered the hygric capacity of the air inside the greenhouse (the ω factor of Eq. (9) was set equal to one). This choice was because no

reliable data concerning the moisture buffer value of greenhouse are available in literature, therefore the estimation of the final value of ω is performed through the calibration process.

The results of the optimisation process that are then used for the calibrated simulation for the model validation are presented in Table 4. In the first instance, the *LAI* was considered equal to 0.4 m^2 m^{-2} at the beginning of the production cycle and 1.6 m^2 m^{-2} at the end of it. The optimization process changed those values and in the calibrated model the *LAI* is equal to 0.15 m^2 m^{-2} at the beginning of the production cycle and 1.14 m^2 m^{-2} at the end of it.

4.4. Model validation

4.4.1. Goodness-of-fit indexes

The presented model is validated comparing the results carried out through a calibrated simulation with the data acquired through the monitoring campaign.

The differences in terms of θ_{air_i}, RH_i and E_{el} between the measured and the estimated values are evaluated using two different goodness-of-fit indices that are calculated with an hourly basis. The first index is the Mean Bias Error (*MBE*) that reads

$$MBE = \frac{\sum_{j=1}^{n_{set}} \left(\widetilde{\chi}_j - \chi_j \right)}{\sum_{j=j}^{n_{set}} \widetilde{\chi}_i} \cdot 100 \quad [\%] \tag{30}$$

where χ_j and $\widetilde{\chi}_j$ are the simulated and measured values at the hourly time-step j, respectively, while n_{set} is the number of hourly values considered in the validation period.

The other chosen calculated goodness-of-fit index is the Coefficient of variation of the *RMSE* (*Cv(RMSE)*) that reads

$$Cv(RMSE) = \frac{RMSE}{\left(\sum_{j=1}^{n_{set}} \widetilde{\chi}_j \right) \cdot \frac{1}{n_{set}}} \cdot 100 \quad [\%] \tag{31}$$

where *RMSE* is the Root Mean Square Error calculated similarly to Eq. (22).

The reliability of the model in estimating the electrical energy consumption due to dehumidification and cooling ventilation over long periods of simulation is estimated also considering the deviation of the simulated energy consumption from the monitored one (ΔE_{el}) over the validation period as

$$\Delta E_{el} = \frac{\left(\sum_{j=1}^{n_{set}} \chi_j \right) - \left(\sum_{j=1}^{n_{set}} \widetilde{\chi}_j \right)}{\left(\sum_{j=1}^{n_{set}} \widetilde{\chi}_j \right)} \quad [\%] \tag{32}$$

4.4.2. Validation results

In Fig. 14 the hourly trends of simulated values of θ_{air_i}, RH_i and E_{el} are displayed against the measured ones during the validation period. In addition, the monitored values of θ_{air_o} and RH_o are also displayed. During the considered period (July), both θ_{air_o} and RH_o are

Table 4
Values of the calibration parameters after the solution of the optimisation problem.

Coefficient	Value [-]
γ_{glass}	1.25
γ_{floor}	0.99
γ_{th}	3.83
γ_{m_LAI}	0.82
γ_{q_LAI}	0.36
γ_{hig}	1.48

characterised by considerably high values. In particular, θ_{air_o} ranges between 17.1 and 33.2 °C, while RH_o values are between 50 and 90%. These outdoor air external conditions entail high values of θ_{air_i} and RH_i and, consequently, high E_{el} due to fan activation.

Fig. 14 shows that the model is reliable (from a qualitative point of view) in estimating the indoor environmental conditions and electrical energy consumption of the monitored greenhouse. The measured and simulated trends of θ_{air_i} (Fig. 14a) are very similar between them, especially during nighttime, when θ_{air_i} is in free-floating conditions due to the absence of solar radiation and the lower value of θ_{air_o} (no cooling is needed). During daytime, the higher θ_{air_o} and the presence of solar radiation cause the activation of the installed fans (as visible from the E_{el} trends of Fig. 14c) and slight differences between the two θ_{air_i} trends (the measured and simulated ones) stand out. These differences are especially evident on July 9th and 10th when (at around 12:00) the simulated θ_{air_i} suddenly decreases while the measured θ_{air_i} follows rising. This discrepancy is due to slight differences in the modelling of the evaporative cooling system.

The difference in evaporative pad activation also explains the small spikes that characterize the simulated trend of θ_{air_i} that have a major effect the trend of simulated RH_i, showed in Fig. 14b. The simulated RH_i trend, in fact, is characterized by spikes that are not present in the measured one. Those spikes are caused by the sudden activation of the evaporative cooling pads that enhances the inlet of fresh saturated cool air inside the greenhouse. The inlet of this air causes a consequent decrease of θ_{air_i} (as visible in Fig. 14a) that reflects in the sudden increase of RH_i. In addition, it has to be considered the incoming air is characterized by a high x_{air_sup} (due to the adiabatic cooling process that takes place inside the pads) that increases x_{air_i} and, consequently, RH_i. The RH_i spikes are present in the trend estimated by model since it considers that the pads are activated/deactivated with an hourly time step. In the real greenhouse the situation is quite different since pads are activated/deactivated with sub-hourly time steps, avoiding the presence of similar spikes in the monitored trend.

Fig. 14c shows the comparison between the simulated and measured hourly E_{el} due to fan activation. As visible from the chart, the main difference between the measured and simulated energy trends regards the maximum of energy consumption that is achieved daily. The measured E_{el}, in fact, achieves a maximum daily value higher than the simulated E_{el}. This difference is slight (less than 1 kWh) and it seems a sort of systematic error since it is appreciable during most of the days of the validation period, except July 10th, 11th, 12th, and 18th. This systematic error could be ascribable to a slight difference between the fan implemented in the energy model and the real ones installed in the monitored greenhouse. This difference may be due how the fan was implemented in the energy model or due some discrepancies between the specifications reported in the technical datasheet of the fans and their real performance once installed on field.

Another interesting element that stands out from the analysis of Fig. 14c is the trend of both monitored and simulated E_{el} on July 11th and 12th that is considerably different from the other days. This difference is due to the θ_{air_o} values (visible in Fig. 14a) that, on July 11th and 12th, is at the minimum values of the analysed period. The cooler θ_{air_o} makes it possible to maintain θ_{set_C} (27.7 °C) without activating cooling ventilation. Therefore, during July 11th and 12th only dehumidification ventilation was activated, requiring a lower electrical power.

The reliability of the model that is proved from a qualitative point of view by Fig. 14, is also analysed from a quantitative point of view comparing the calculated *MBE* and *Cv(RMSE)* with the main thresholds for validating energy simulation models for buildings through calibrated simulations, as recommended in [82]. The sources of thresholds considered in this work are:

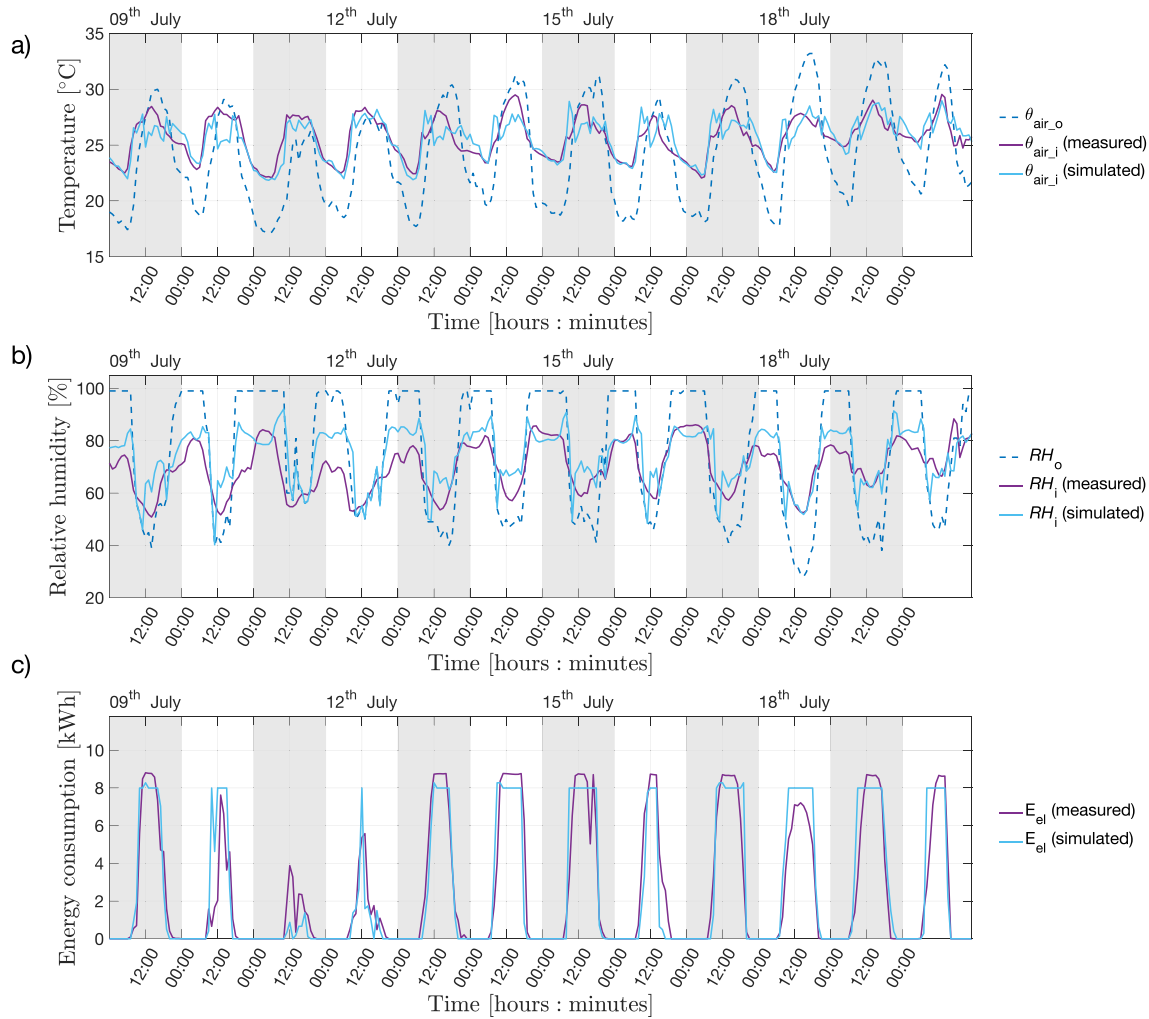- American Society of Heating, Refrigerating and Air-Conditioning Engineers (ASHRAE) Guidelines 14 [86];

Fig. 14. Trends of monitored and simulated values of (a) indoor air temperature (θ_{air_i}), (b) relative humidity (RH_i), (c) and hourly electrical energy consumption. The outdoor air temperature (θ_{air_o}) and relative humidity (RH_o) are also showed.

- International Performance Measurements and Verification protocol (IPMVP) [87];
- Federal Energy Management Program (FEMP) Measurements and Verification (M&V) guidelines [88];

In Table 5, the values of *MBE* and *Cv*(*RMSE*) for θ_{air_i}, RH_i and E_{el} calculated before and after the calibration are shown together with the respective threshold values for hourly validation. In addition, the *RMSE* is also presented since even though ASHRAE Guidelines 14 [86], IPMVP [87] and FEMP [88] do not provide threshold values for this index, it

Table 5
Values (before and after the calibration) of goodness-of-fit indices and threshold values for the hourly validation of the presented energy simulation model, concerning indoor air temperature (θ_{air_i}), relative humidity (RH_i) and hourly electrical energy consumption (E_{el}).

Parameter	Goodness-of-fit index	Calculated value		Thresholds value (hourly validation)		
		Before calibration	After calibration	ASHRAE [86]	IPMVP [87]	FEMP [88]
	MBE[a]	0.7%	0.3%	±10%	±5%	±10%
θ_{air_i}	*Cv*(*RMSE*)[b]	5.2%	4.5%	30%	20%	30%
	RMSE[c]	1.35 °C	1.16 °C	–	–	–
	MBE	−10.6%	−6.1%	±10%	±5%	±10%
RH_i	*Cv*(*RMSE*)	18.2%	13.1%	30%	20%	30%
	RMSE	12.7%	9.1%	–	–	–
	MBE	−33.2%	−1.2%	±10%	±5%	±10%
E_{el}	*Cv*(*RMSE*)	83.7%	55.3%	30%	20%	30%
	RMSE	2.04 kWh	1.35 kWh	–	–	–

[a] Mean Bias Error.
[b] Coefficient of Variation of the Root Mean Square Error.
[c] Root Mean Square Error.

represents a good measure of the extent of the error between the estimated trend and the simulated one. Please note that the goodness-of-fit indices reported in Table 5 were calculated considering the hours of the validation period only. The hours that were used for the model calibration were not considered for the calculation of those indices.

The values reported in Table 5 show that the calculated goodness-of-fit indices respect all the considered threshold values for both θ_{air_i} and RH_i (even the most restrictive ones from IPMVP), while E_{el} does not respect only the $Cv(RMSE)$ thresholds. The $RMSE$ is equal to 1.16 °C for θ_{air_i} and 9.1% for RH_i demonstrating that the error of the model in estimating these two indoor environmental parameters is small during the validation period, confirming the reliability of the presented model. The obtained $RMSE$ are similar to the ones found in other similar works in the literature [7,41]. The $RMSE$ for E_{el} is 1.35 kWh a value that would further decrease if the systematic error that was highlighted in Fig. 14c is not considered. This error could appear slightly high, but it should be considered that the developed model adopts an hourly simulation time step. To improve the energy consumption prediction, lower simulation time steps should be adopted to improve the simulation of the dynamics of fan activation. Nevertheless, lower simulation time steps would increase the computation time reducing the usability of the model.

The reliability of the model from the energy point over long periods of simulation can be also evaluated comparing the simulated and measured energy consumptions over the entire validation period. The model, in fact, estimates an electrical energy consumption for dehumidification and cooling ventilation of 711 kWh, while the monitoring campaign provided an electrical energy consumption of 703 kWh. According to the formulation of Eq. (32), a ΔE_{el} of roughly can be calculated 1.1%, meaning that there is just a slight overestimation of the electrical energy consumption. The model estimates that during the validation period no thermal energy was needed to heat the enclosure, a result that is confirmed by the monitoring campaign in which, the heating system was not operative.

The previous analyses show that the model is reliable for the purpose of this work and it can be adopted to perform long term simulations considering different configurations of the greenhouse systems at both the envelope and system levels to find the best configuration for improving the greenhouse energy performance. An example of model application is presented in the following section.

5. Model application

The potentialities of the presented energy simulation model are several since it enhances the possibility to simulate different types of greenhouses in different climate conditions and specially to evaluate the effect of different types of control systems and new equipment. The results provide interesting information about the indoor environmental conditions and the related energy performance.

To exploit the potentialities of the presented model, the greenhouse described in Section 4.2.1 is simulated in three different scenarios considering the climate conditions of three different locations presented in Table 6 (data from the Test Meteorological Year).

In Fig. 15, the absolute and cumulative frequencies of the simulated

Table 6
Outdoor climate conditions used to perform the simulations.

Scenario	Location	θ_{air_o}(average)[a]	Annual solar radiation[b]
Verona (Italy)	Southern Europe	12.3 °C	1070 kWh m^{-2}
Seville (Spain)	Southwestern Europe	18.4 °C	1769 kWh m^{-2}
Nantes (France)	Northwestern Europe	12.2 °C	1180 kWh m^{-2}

[a] Value calculated considering the hourly values of the entire TMY.
[b] Value referring to the total outdoor solar radiation on horizontal surface.

θ_{air_i} for the three climate scenarios are presented. The frequencies of Verona and Nantes scenarios are quite similar between them, while important differences stand out comparing those climate scenarios with the Sevilla one. Verona and Nantes scenarios, in fact, are characterized by a higher frequency of lower θ_{air_i} since the cumulative frequency of the class 20 °C is higher than 70% in both the climate scenarios. On the contrary, in Sevilla scenario higher temperatures can be observed and the cumulative frequency of 20 °C is 50%, considerably lower than in the other considered climate scenarios. This different distribution of θ_{air_i} frequency will reflect also in different thermal and electrical energy consumption that are showed later in the text.

The absolute frequency distributions presented in Fig. 15 show that θ_{air_i} is always higher than 14 °C. The most frequent value of θ_{air_i} is 16 °C for all the climate scenarios and its absolute frequency ranges between around 2100 (Seville) and 3200 (Nantes). This high absolute frequency is explained considering that 16 °C is the set point temperature that is maintained by the climate control system during the day. During nighttime, the climate control system maintains a setback temperature of 14 °C. Consequently, 14 and 16 °C are characterized by very high absolute frequencies. On the contrary, 15 °C has a very low absolute frequency since this θ_{air_i} value can occur only in certain conditions during nighttime and in those hours in which θ_{air_i} increases from 14 to 16 °C and vice versa.

In Fig. 16, the cumulative electrical and thermal energy consumption for heating and ventilation in the simulated climate scenarios are presented. Fig. 16a shows that the higher electrical energy consumption is from Seville scenario where the warm outdoor weather conditions entail a considerably electrical energy consumption for fan activation (10,180 kWh$_{el}$, 6.02 kWh$_{el}$ m^2). That energy consumption value is considerably higher than the ones of Verona (2161 kWh$_{el}$, 1.28 kWh$_{el}$ m^2) and Nantes (534 kWh$_{el}$, 0.32 kWh$_{el}$ m^2).

An opposite trend regards the thermal energy consumption, as visible from Fig. 16b. Seville scenario, in fact, is characterised by a yearly thermal energy consumption of 57,063 kWh$_{th}$ (around 33.77 kWh$_{th}$ m^2) a value considerably lower than the one found for Nantes scenario (199,397 kWh$_{th}$, around 117.99 kWh$_{th}$ m^2) and Verona one (269,528 kWh$_{th}$, around 159.48 kWh$_{th}$ m^2).

The presented results agree with other studies present in scientific literature that underline how most of the energy consumption of greenhouse is due to space heating [12,14]. For this reason, future investigations should aim at reducing heating energy consumption exploiting energy simulation tools such the one presented in this work. In particular, the estimated thermal energy consumption results considerably higher than the one of other agricultural building characterised by high values of energy consumption for climate control, such as intensive livestock houses [89].

The previously presented electrical energy consumptions were estimated considering variable angular speed fans installed in the simulated greenhouse (as described in Section 4.2.1). In Table 7, the previously obtained electrical energy consumption are compared with the ones that were obtained considering a set of 15 fixed angular speed fans of 0.56 kW (0.75 hp) and 19,100 m^3 h^{-1} of maximum flow rate installed in the greenhouse, as it can be observed in many existing structures. As visible from the table, variable angular speed fans entail a decrease of the electrical energy consumption for ventilation between 24 and 34% if compared with fixed angular speed fans.

6. Conclusions

In this work a coupled first-principle dynamic energy simulation model for the calculation of energy consumption and indoor environmental conditions of fully mechanically ventilated greenhouses was elaborated and presented. After a monitoring campaign for the acquisition of the dataset, the model was validated through calibrated simulations. The results were evaluated in compliance with the main
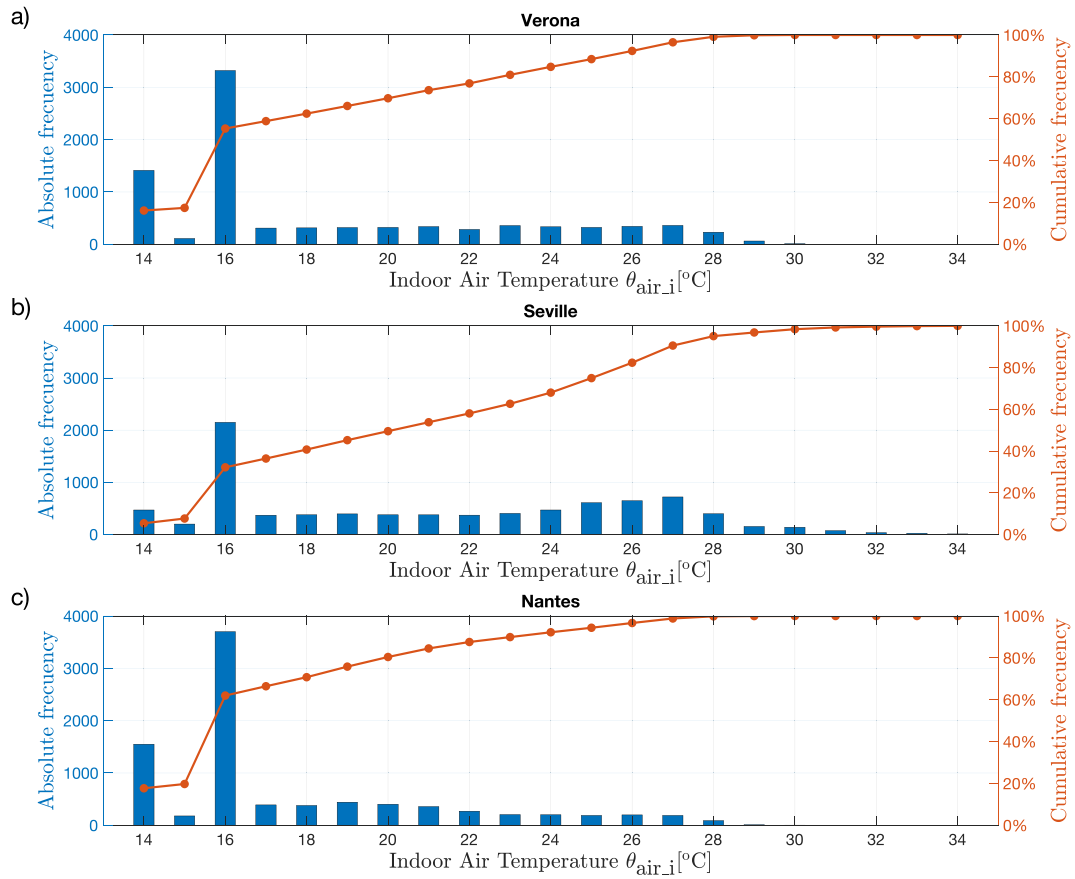
Fig. 15. Absolute and cumulative frequencies of indoor air temperature for the considered scenarios of Verona (a), Seville (b) and Nantes (c).
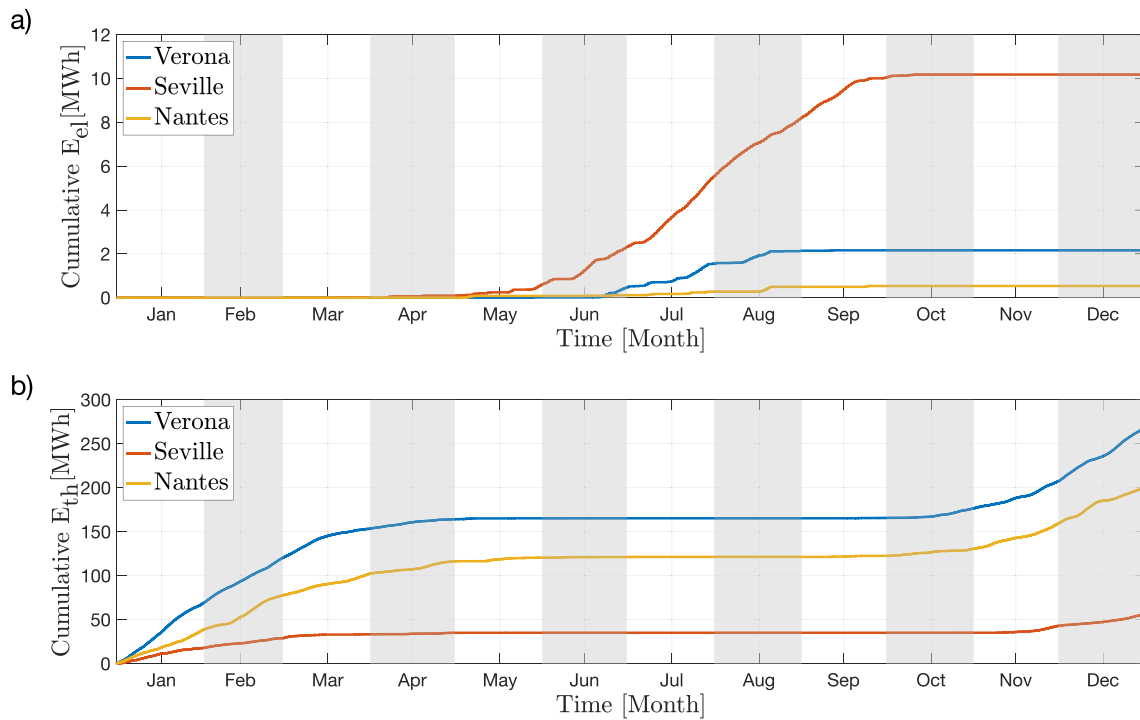

Fig. 16. Cumulative electrical (a) and thermal (b) energy consumption for the considered climate scenarios.

Table 7

Comparison between electrical energy consumption for ventilation considering variable and fixed angular speed fans.

Scenario	E_{el} (variable angular speed fans)	E_{el} (fixed angular speed fans)	Energy saving due to variable angular speed fans
Verona (Italy)	2161 kWh$_{el}$	2958 kWh$_{el}$	−27%
Seville (Spain)	10,180 kWh$_{el}$	13,441 kWh$_{el}$	−24%
Nantes (France)	534 kWh$_{el}$	810 kWh$_{el}$	−34%

protocols for building energy simulation present in literature. The model proved to be reliable in providing the estimation of time profiles of the indoor air temperature and relative humidity in accordance with those measured in the experimentation. The model also properly estimates the electrical energy consumption for dehumidification and cooling ventilation.

The main strength of the presented model lies in its integrated approach in simulating the greenhouse dynamics (e.g. thermal and hygric behaviour of the building) and the consequent dynamic response of the climate control systems. The presented energy model integrates the most adopted climate control equipment in large multi-span greenhouses, including the new variable angular speed fans, a promising energy-efficient technology for greenhouses that has yet to be exploited in this sector. Integration of such fans in this simulation model, represents a novelty in literature.

The presented model could represent a decision support tool for the stakeholders in the energy design and retrofit stage of fully-mechanically ventilated greenhouses. Stakeholders, in fact, will use this energy simulation model to create a greenhouse "digital mock-up" to test a wide range of configuration creating scenarios characterized by different solutions with different solutions at both envelope and system level, by different features production cycle (e.g. cultivated crop and cycle length), and by different settings of climate control system (e.g. set point temperatures and minimum ventilation). The results of those simulations could lead stakeholders to adopt the most energy-efficient solution to improve the energy performance for climate control of greenhouses. An example of the application of this model was presented in this work, considering various solutions at system level (variable and fixed angular speed fans) in different outdoor climate conditions.

Further improvements and fine-tuning calibrations could convert the presented model also in a digital twin of existing greenhouses, providing analytics useful for improving the greenhouse management and further improving the energy performance during the operational stage. Future model improvements may integrate additional equipment for climate control, new technologies and new calculation modules for different purposes (e.g. simulation of natural ventilation, the estimation of on-site energy renewable energy production and the assessment of greenhouse gas emissions).

CRediT authorship contribution statement

Andrea Costantino: Data curation, Formal analysis, Investigation, Methodology, Resources, Software, Validation, Visualization, Writing – review & editing. **Lorenzo Comba:** Data curation, Investigation, Methodology, Resources, Visualization, Writing – review & editing. **Giacomo Sicardi:** Data curation, Formal analysis, Investigation, Software, Validation, Visualization, Writing – original draft. **Mauro Bariani:** Conceptualization, Project administration, Resources. **Enrico Fabrizio:** Conceptualization, Funding acquisition, Investigation, Methodology, Project administration, Resources, Supervision, Writing – review & editing.

Declaration of Competing Interest

The authors declare that they have no known competing financial interests or personal relationships that could have appeared to influence the work reported in this paper.

Acknowledgements

Appendix A. Set of equations for thermal balance solution

To calculate $\phi_{H/C,nd}$, the equivalent electrical network is solved with an hourly time discretization according to a Cranck-Nicholson time scheme.

To simplify the equations, the above reported heat transfer coefficients are grouped into H_{tr_1}, H_{tr_2}, and H_{tr_3}, as described in paragraph C.3 of Annex C of ISO 13790 [67], where the complete set of equations of the adopted method is contained. For the j-th time-step, the network has to be solved to calculate the value of the $\theta_{air\_i,j}$ considering as mass temperature $\theta_{m,j-1}$, referred to previous time-step. The calculation is performed through the following equations

$$\theta_{m,j} = \frac{\theta_{m,j-1} \cdot \left[\frac{C_{gh}}{3600} - 0.5 \cdot (H_{tr\_3} + H_{tr\_em}) \right] + \phi_{m\_tot,j}}{\frac{C_{gh}}{3600} + 0.5 \cdot (H_{tr\_3} + H_{tr\_em})} \quad [°C] \tag{A.1}$$

where $\phi_{m\_tot,j}$ represents the whole heat flow occurring in the hourly time-step (calculated according to [67]) and C_{gh} is the building fabric heat capacity (J K^{-1});

$$\theta_m = \frac{\theta_{m,j} + \theta_{m,j-1}}{2} \quad [°C] \tag{A.2}$$

$$\theta_{s,j} = \frac{H_{tr\_ms} \cdot \theta_m + \phi_{st} + H_{tr\_fen} \cdot \theta_{air\_o} + H_{tr\_1} \cdot \left(\theta_{air\_sup} + \frac{\phi_{ia} + \phi_{H/C\_nd}}{H_{ve}} \right)}{H_{tr\_ms} + H_{tr\_fen} + H_{tr\_1}} \quad [°C] \tag{A.3}$$

in Eq. (A.3), θ_{air_o} is used instead of θ_{air_sup} when evaporative pads are not activated;

$$\theta_{\text{air\_i,j}} = \frac{H_{\text{tr\_is}} \cdot \theta_{\text{s}} + H_{\text{ve}} \cdot \theta_{\text{air\_sup}} + \phi_{\text{ia}} + \phi_{\text{H/C\_nd}}}{H_{\text{tr\_is}} + H_{\text{ve}}} \quad [°\text{C}] \tag{A.4}$$

To determine if the air temperature $\theta_{\text{air\_i,j}}$ is within the range $\theta_{\text{set\_H}}$ and $\theta_{\text{set\_C}}$, and to compute the possible required thermal load $\phi_{\text{H/C,nd}}$, Eqs. (A.1-A.4) are performed twice for each time-step *j*, imposing the following two values of $\phi_{\text{H/C,nd}}$:

- $\phi_{\text{H/C\_nd}} = 0$ W m^{-2};
- $\phi_{\text{H/C\_nd}} = 10$ W m^{-2}.

The air temperature calculated imposing $\phi_{\text{H/C,nd}}$ equal to 0 W m^{-2} is named $\theta_{\text{air\_i(0)}}$, while when it is calculated imposing $\phi_{\text{H/C,nd}}$ equal to 10 W m^{-2} is named $\theta_{\text{air\_i(10)}}$. At this stage of calculation, two different situations can occur:

1. if $\theta_{\text{air\_i(0)}}$ stays within $\theta_{\text{set\_H}}$ and $\theta_{\text{set\_C}}$, the building does not require neither supplemental heating nor cooling ($\phi_{\text{H/C\_nd}} = 0$ W m^{-2}) and $\theta_{\text{air\_i}}$ is in free-floating conditions;
2. if $\theta_{\text{air\_i(0)}}$ falls out of the range ($\theta_{\text{set\_H}} - \theta_{\text{set\_C}}$), $\phi_{\text{H/C\_nd}}$ is calculated as

$$\phi_{\text{H/C\_nd}} = \phi_{\text{H/C\_nd(10)}} \cdot \frac{\theta_{\text{set\_H/C}} - \theta_{\text{air\_i(0)}}}{\theta_{\text{air\_i(10)}} - \theta_{\text{air\_i(0)}}} \quad [\text{W}] \tag{A.5}$$

where $\phi_{\text{H/C\_nd(10)}}$ is the heating or cooling load calculated considering 10 W m^{-2}.

References

[1] United Nations. World population prospects 2019: Highlights; 2019.

[2] Janke RR, Altamimi ME, Khan M. The use of high tunnels to produce fruit and vegetable crops in North America. Agric Sci 2017;8:692–715. https://doi.org/10.4236/as.2017.87052.

[3] Iddio E, Wang L, Thomas Y, McMorrow G, Denzer A. Energy efficient operation and modeling for greenhouses: a literature review. Renew Sustain Energy Rev 2020;117:109480. https://doi.org/10.1016/j.rser.2019.109480.

[4] Critten DL, Bailey BJ. A review of greenhouse engineering developments during the 1990s. Agric For Meteorol 2002;112:1–22. https://doi.org/10.1016/S0168-1923(02)00057-6.

[5] Albright LD, Reines RG, Anderson SE, Chandra P, Price DR. Experimental results of solar heating a brace institute style greenhouse. Proc third annu conf sol energy heat greenhouses. 1978.

[6] McCartney L, Lefsrud MG. Protected agriculture in extreme environments: a review of controlled environment agriculture in tropical, arid, polar, and urban locations. Appl Eng Agric 2018;34:455–73. https://doi.org/10.13031/aea.12590.

[7] Taki M, Ajabshirchi Y, Ranjbar SF, Rohani A, Matloobi M. Modeling and experimental validation of heat transfer and energy consumption in an innovative greenhouse structure. Inf Process Agric 2016;3:157–74. https://doi.org/10.1016/j.inpa.2016.06.002.

[8] Vadiee A, Martin V. Energy management strategies for commercial greenhouses. Appl Energy 2014;114:880–8. https://doi.org/10.1016/j.apenergy.2013.08.089.

[9] Khoshnevisan B, Shariati HM, Rafiee S, Mousazadeh H. Comparison of energy consumption and GHG emissions of open field and greenhouse strawberry production. Renew Sustain Energy Rev 2014;29:316–24. https://doi.org/10.1016/j.rser.2013.08.098.

[10] De Villiers DS, Wien HC, Reid JE, Albright LD. Energy use and yields in tomato production: Field, high tunnel and greenhouse compared for the northern tier of the USA (Upstate New York). Acta Hortic 2011;893:373–80. https://doi.org/10.17660/ActaHortic.2011.893.34.

[11] IEA. World energy balances – 2019 edition – Database documentation; 2019.

[12] Kittas C, Katsoulas N, Bartzanas T, Bakker S. Greenhouse climate control and energy use. In: Baudoin W, Nono-Womdim R, Lutaladio N, Hodder A, Castilla N, Leonardi C, et al., editors. Good agric pract greenh veg crop, Rome: FAO; 2013.

[13] The Carbon Trust. CT009 Agriculture and Horticulture – Sector Overview. London (UK); 2012.

[14] Runkle E, Both AJ. Greenhouse energy conservation strategies. Extention Bull 2011:1–16. https://doi.org/10.7282/T3K64KWN.

[15] Xu J, Li Y, Wang RZ, Liu W, Zhou P. Experimental performance of evaporative cooling pad systems in greenhouses in humid subtropical climates. Appl Energy 2015;138:291–301. https://doi.org/10.1016/j.apenergy.2014.10.061.

[16] Firfiris VK, Fragos VP, Kotsopoulos TA, Nikita-Martzopoulou C. Energy and environmental analysis of an innovative greenhouse structure towards frost prevention and heating needs conservation. Sustain Energy Technol Assess 2020;40:100750. https://doi.org/10.1016/j.seta.2020.100750.

[17] Yang SH, Rhee JY. Utilization and performance evaluation of a surplus air heat pump system for greenhouse cooling and heating. Appl Energy 2013;105:244–51. https://doi.org/10.1016/j.apenergy.2012.12.038.

[18] Bibbiani C, Fantozzi F, Gargari C, Campiotti CA, Schettini E, Vox G. Wood biomass as sustainable energy for greenhouses heating in Italy. Agric Agric Sci Procedia 2016;8:637–45. https://doi.org/10.1016/j.aaspro.2016.02.086.

[19] Sethi VP, Sumathy K, Lee C, Pal DS. Thermal modeling aspects of solar greenhouse microclimate control: a review on heating technologies. Sol Energy 2013;96:56–82. https://doi.org/10.1016/j.solener.2013.06.034.

[20] EN. Greenhouses – Design and construction – Part 1: Commercial production greenhouses; 2019.

[21] Ward R, Mortada A, Choudhary R. Simulation of thermal performance and retrofit of a historic greenhouse. In: Mahdavi A, Martens B, editors. Proc from 2nd cent eur symp build phys; 2013. p. 245–52.

[22] Ahamed MS, Guo H, Tanino K. Modeling heating demands in a Chinese-style solar greenhouse using the transient building energy simulation model TRNSYS. J Build Eng 2020;29:101114. https://doi.org/10.1016/j.jobe.2019.101114.

[23] CERES – Greenhouse solutions. An introduction to vapor pressure deficit; 2018. https://ceresgs.com/an-introduction-to-vapor-pressure-deficit/ [accessed October 20, 2020].

[24] Comba L, Biglia A, Ricauda Aimonino D, Tortia C, Mania E, Guidoni S, et al. Leaf area index evaluation in vineyards using 3D point clouds from UAV imagery. Precis Agric 2020;21:881–96. https://doi.org/10.1007/s11119-019-09699-x.

[25] Hellickson MAMA, Walker JNJN. Ventilation of agricultural structures. St. Joseph: ASAE; 1983.

[26] Chen J, Xu F, Ding B, Wu N, Shen Z, Zhang L. Performance analysis of radiation and electricity yield in a photovoltaic panel integrated greenhouse using the radiation and thermal models. Comput Electron Agric 2019;164:104904. https://doi.org/10.1016/j.compag.2019.104904.

[27] Lando I, Serale G, Fabrizio E. Dynamic thermal modelling of a large plastic multi-span greenhouse: calibrated simulation and energy retrofit. ASABE 2018 annu int meet. 2018.

[28] Campbell CD, Sage RF, Kocacinar F, Way DA. Estimation of the whole-plant CO2 compensation point of tobaco (Nicotiana tabacum L.). Glob Chang Biol 2005;11:1956–67. https://doi.org/10.1111/j.1365-2486.2005.01045.x.

[29] Nederhoff E. Carbon dioxide enrichment – fuels & figures. Pract Hydroponics Greenhouses. May/June:50–9.

[30] Singh MC, Singh JPP, Singh KGG. Development of a microclimate model for prediction of temperatures inside a naturally ventilated greenhouse under cucumber crop in soilless media. Comput Electron Agric 2018;154:227–38.

[31] Golzar F, Heeren N, Hellweg S, Roshandel R. A novel integrated framework to evaluate greenhouse energy demand and crop yield production. Renew Sustain Energy Rev 2018;96:487–501. https://doi.org/10.1016/j.rser.2018.06.046.

[32] Van Beveren PJM, Bontsema J, Van Straten G, Van Henten EJ. Minimal heating and cooling in a modern rose greenhouse. Appl Energy 2015;137:97–109. https://doi.org/10.1016/j.apenergy.2014.09.083.

[33] van Beveren PJM, Bontsema J, van Straten G, van Henten EJ. Optimal control of greenhouse climate using minimal energy and grower defined bounds. Appl Energy 2015;159:509–19. https://doi.org/10.1016/j.apenergy.2015.09.012.

[34] Lin D, Zhang L, Xia X. Hierarchical model predictive control of Venlo-type greenhouse climate for improving energy efficiency and reducing operating cost. J Clean Prod 2020;264:121513. https://doi.org/10.1016/j.jclepro.2020.121513.

[35] Chen J, Yang J, Zhao J, Xu F, Shen Z, Zhang L. Energy demand forecasting of the greenhouses using nonlinear models based on model optimized prediction method. Neurocomputing 2016;174:1087–100. https://doi.org/10.1016/j.neucom.2015.09.105.

[36] Altes-Buch Q, Quoilin S, Greenhouses Lemort V. A modelica library for the simulation of greenhouse climate and energy systems. In: Proc 13th int model conf regensburg, ger March 4–6 2019; 2019. https://doi.org/10.3384/ecp19157533.

[37] Taki M, Rohani A, Rahmati-Joneidabad M. Solar thermal simulation and applications in greenhouse. Inf Process Agric 2018;5:83–113. https://doi.org/10.1016/j.inpa.2017.10.003.

[38] Mobtaker HG, Ajabshirchi Y, Ranjbar SF, Matloobi M. Simulation of thermal performance of solar greenhouse in north-west of Iran: an experimental validation. Renew Energy 2019;135:88–97.

[39] Joudi KA, Farhan AA. A dynamic model and an experimental study for the internal air and soil temperatures in an innovative greenhouse. Energy Convers Manag 2015;91:76–82. https://doi.org/10.1016/j.enconman.2014.11.052.

[40] Reyes-Rosas A, Molina-Aiz FD, Valera DL, López A, Khamkure S. Development of a single energy balance model for prediction of temperatures inside a naturally ventilated greenhouse with polypropylene soil mulch. Comput Electron Agric 2017;142:9–28. https://doi.org/10.1016/j.compag.2017.08.020.

[41] Zhang G, Ding X, Li T, Pu W, Lou W, Hou J. Dynamic energy balance model of a glass greenhouse: an experimental validation and solar energy analysis. Energy 2020;198:117281. https://doi.org/10.1016/j.energy.2020.117281.

[42] Brown J, Ward R, Choudhary R, Slater R. Algorithmic and declarative modeling of a greenhouse. In: Proc 5th int build phys conf; 2012. p. 577–84.

[43] Jans-Singh MK, Ward R, Choudhary R. Co-simulation of a rooftop greenhouse and a school building in London, UK. In: Proc build simul 2019 16th conf IBPSA; 2020. https://doi.org/10.26868/25222708.2019.210355.

[44] Gholami M, Barbaresi A, Tassinari P, Bovo M, Torreggiani D. A comparison of energy and thermal performance of rooftop greenhouses and green roofs in mediterranean climate: a hygrothermal assessment in WUFI. Energies 2020;13:2030. https://doi.org/10.3390/en13082030.

[45] del Sagrado J, Sánchez JA, Rodríguez F, Berenguel M. Bayesian networks for greenhouse temperature control. J Appl Log 2016;17:25–35. https://doi.org/10.1016/j.jal.2015.09.006.

[46] Taki M, Abdanan Mehdizadeh S, Rohani A, Rahnama M, Rahmati-Joneidabad M. Applied machine learning in greenhouse simulation; new application and analysis. Inf Process Agric 2018;5:253–68. https://doi.org/10.1016/j.inpa.2018.01.003.

[47] Blasco X, Martínez M, Herrero JM, Ramos C, Sanchis J. Model-based predictive control of greenhouse climate for reducing energy and water consumption. Comput Electron Agric 2007;55:49–70. https://doi.org/10.1016/j.compag.2006.12.001.

[48] Zhou N, Yu Y, Yi J, Liu R. A study on thermal calculation method for a plastic greenhouse with solar energy storage and heating. Sol Energy 2017;142:39–48. https://doi.org/10.1016/j.solener.2016.12.016.

[49] Jolliet O, Danloy L, Gay JB, Munday GL, Reist A. HORTICERN: an improved static model for predicting the energy consumption of a greenhouse. Agric For Meteorol 1991;55:265–94. https://doi.org/10.1016/0168-1923(91)90066-Y.

[50] Singh RD, Tiwari GN. Energy conservation in the greenhouse system: a steady state analysis. Energy 2010;35:2367–73. https://doi.org/10.1016/j.energy.2010.02.003.

[51] Campiotti C, Latini A, Scoccianti M, Viola C. L'ottenimento dei Certificati Bianchi. La scheda 40 E: I sistemi serra; 2014. [in Italian].

[52] Ahamed MS, Guo H, Tanino K. A quasi-steady state model for predicting the heating requirements of conventional greenhouses in cold regions. Inf Process Agric 2018;5:33–46. https://doi.org/10.1016/j.inpa.2017.12.003.

[53] Chen C, Yu N, Yang F, Mahkamov K, Han F, Li Y, et al. Theoretical and experimental study on selection of physical dimensions of passive solar greenhouses for enhanced energy performance. Sol Energy 2019;191:46–56. https://doi.org/10.1016/j.solener.2019.07.089.

[54] Rasheed A, Na WH, Lee JW, Kim HT, Lee HW. Optimization of greenhouse thermal screens for maximized energy conservation. Energies 2019;12:3592. https://doi.org/10.3390/en12193592.

[55] Bambara J, Athienitis AK. Energy and economic analysis for greenhouse envelope design. Trans ASABE 2018;61:1795–810. https://doi.org/10.13031/trans.13025.

[56] Costantino A, Fabrizio E, Ghiggini A, Bariani M. Climate control in broiler houses: a thermal model for the calculation of the energy use and indoor environmental conditions. Energy Build 2018;169:110–26.

[57] Duffie JA, Beckman WA. Solar engineering of thermal processes: 4th ed.; 2013. https://doi.org/10.1002/9781118671603.

[58] Adeyemi O, Grove I, Peets S, Domun Y, Norton T. Dynamic modelling of lettuce transpiration for water status monitoring. Comput Electron Agric 2018;155:50–7. https://doi.org/10.1016/j.compag.2018.10.008.

[59] Stanghellini C. Transpiration of greenhouse crops an aid to climate management. Agric Eng 1987.

[60] Penman HL. Natural evaporation from open water, bare soil and grass. Proc R Soc 1948;193.

[61] Monteith JL. Photosynthesis and transpiration of crops. Exp Agric 1966;2:1–14. https://doi.org/10.1017/s0014479700003938.

[62] Li L, Chen S, Yang C, Meng F, Sigrimis N. Prediction of plant transpiration from environmental parameters and relative leaf area index using the random forest regression algorithm. J Clean Prod 2020;261:121136. https://doi.org/10.1016/j.jclepro.2020.121136.

[63] Boulard T, Wang S. Greenhouse crop transpiration simulation from external climate conditions. Agric For Meteorol 2000;100:25–34. https://doi.org/10.1016/S0168-1923(99)00082-9.

[64] Villarreal-Guerrero F, Kacira M, Fitz-Rodríguez E, Kubota C, Giacomelli GA, Linker R, et al. Comparison of three evapotranspiration models for a greenhouse cooling strategy with natural ventilation and variable high pressure fogging. Sci Hortic (Amsterdam) 2012. https://doi.org/10.1016/j.scienta.2011.10.016.

[65] Jolliet O. HORTITRANS, a model for predicting and optimizing humidity and transpiration in greenhouses. J Agric Eng Res 1994;57:23–37. https://doi.org/10.1006/jaer.1994.1003.

[66] Marquardt DW. An Algorithm for Least-Squares Estimation of Nonlinear Parameters. J Soc Ind Appl Math 1963;11:431–41. https://doi.org/10.1137/0111030.

[67] European Committee for Standardisation. EN ISO 13790: Energy performance of buildings–Calculation of energy use for space heating and cooling; 2008.

[68] Roujol S, Fleury E, Marchio D, Millet JR, Stabat P, Paris M De, et al. Testing the energy simulation building model of consoclim using bestest method and experimental data. In: Conférence IBPSA World, Eindhoven; 2003. p. 1131–8.

[69] Marchio D, Millet JR, Morisot O. Simple modelling for energy consumption estimation in air conditionned buildings. In: Proc Clima 2000, Brussel, Belgium; 1997.

[70] Costantino A, Ballarini I, Fabrizio E. Comparison between simplified and detailed methods for the calculation of heating and cooling energy needs of livestock housing: a case study. In: Build simul appl, vol. 2017; Febru, 2017. p. 193–200.

[71] ASHRAE. 2012 ASHRAE handbook: HVAC systems and equipment. Atlanta, GA: ASHRAE; 2012.

[72] Munters. CELdek® 7060-15 Evaporative Cooling Pad 2009:2. https://www.munters.com/globalassets/inriver/resources/products/coolers–humidifiers/agh_prodsheet_celdek.pdf [accessed October 20, 2020].

[73] Munters. CELdek® 7090-15 Evaporative Cooling Pad 2011:2. https://www.munters.com/globalassets/inriver/resources/products/coolers–humidifiers/1782-celdek-7090_15_gb.pdf [accessed October 20, 2020].

[74] Guzmán-Cruz R, Castañeda-Miranda R, García-Escalante JJ, López-Cruz IL, Lara-Herrera A, de la Rosa JI. Calibration of a greenhouse climate model using evolutionary algorithms. Biosyst Eng 2009;104:135–42. https://doi.org/10.1016/j.biosystemseng.2009.06.006.

[75] Tap F. Economics-based optimal control of greenhouse tomato crop production. Sn 2000.

[76] Monetti V, Davin E, Fabrizio E, André P, Filippi M. Calibration of building energy simulation models based on optimization: a case study. Energy Procedia 2015;78:2971–6. https://doi.org/10.1016/j.egypro.2015.11.693.

[77] Baker JR, Jones RK. Screening as part of insect and disease management in the greenhouse. North Carolina Flower Grow Bull 1989;34:1–9.

[78] Bailey BJ, Montero JI, Pérez Parra J, Robertson AP, Baeza E, Kamaruddin R. Airflow resistance of greenhouse ventilators with and without insect screens. Biosyst Eng 2003;86:217–29. https://doi.org/10.1016/S1537-5110(03)00115-6.

[79] ASAE. Heating, ventilating, and cooling greenhouses – ANSI/ASAE EP406.4 JAN03; 2003. https://doi.org/10.1016/B978-185617513-5.50030-5.

[80] Ben Ali R, Bouadila S, Mami A. Experimental validation of the dynamic thermal behavior of two types of agricultural greenhouses in the Mediterranean context. Renew Energy 2020;147:118–29. https://doi.org/10.1016/j.renene.2019.08.129.

[81] Costantino A, Comba L, Sicardi G, Bariani M, Fabrizio E. Thermal environment inside mechanically ventilated greenhouses: results from a long-term monitoring campaign. In: Coppola A, Di Renzo GC, Altieri G, D'Antonio P, editors. In: Innov biosyst eng sustain agric for food prod MID-TERM AIIA 2019. Lecture No, Springer; 2020. p. 223–30. https://doi.org/10.1007/978-3-030-39299-4_25.

[82] Fabrizio E, Monetti V. Methodologies and advancements in the calibration of building energy models. Energies 2015;8:2548–74. https://doi.org/10.3390/en8042548.

[83] Comba L, Belforte G, Gay P. Modelling techniques for the control of thermal exchanges in mixed continuous-discontinuous flow food plants. J Food Eng 2011;106:177–87. https://doi.org/10.1016/j.jfoodeng.2011.04.015.

[84] Diago MP, Correa C, Millán B, Barreiro P, Valero C, Tardaguila J. Grapevine yield and leaf area estimation using supervised classification methodology on RGB images taken under field conditions. Sensors (Switzerland) 2012;12:16988–7006. https://doi.org/10.3390/s121216988.

[85] Arnó J, Escolà A, Vallès JM, Llorens J, Sanz R, Masip J, et al. Leaf area index estimation in vineyards using a ground-based LiDAR scanner. Precis Agric 2013;14:290–306. https://doi.org/10.1007/s11119-012-9295-0.

[86] ANSI/ASHRAE. ASHRAE Guideline 14-2002 Measurement of Energy and Demand Savings. Ashrae; 2002.

[87] IPMVP New Construction Subcommittee. International performance measurement & verification protocol: concepts and option for determining energy savings in new construction, vol. III. Washington, DC, USA; 2003.

[88] Federal Energy Management Program. Federal energy management program, M&V guidelines: Measurement and verification for federal energy projects version 3.0; 2008.

[89] Costantino A, Fabrizio E, Biglia A, Cornale P, Battaglini L. Energy use for climate control of animal houses: the state of the art in Europe. Energy Procedia 2016;101:184–91. https://doi.org/10.1016/j.egypro.2016.11.024.